MICROCOPY RESOLUTION TEST CHART

NATIONAL BUREAU OF STANDARDS-1963-A

SIMULATION OF POWDER DISTRIBUTION
IN IITRI BAG EXPERIMENTS

by

Dimitri Gidaspow and M. Syamlal
Department of Chemical Engineering
Illinois Institute of Technology
Chicago, IL 60616

AD-A141 941

84 06 05 150

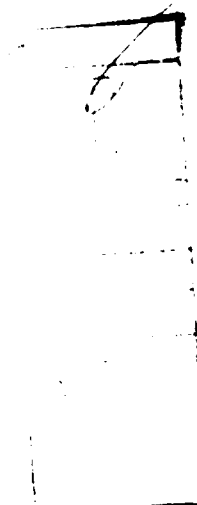# SIMULATION OF POWDER DISTRIBUTION
IN IITRI BAG EXPERIMENTS

by

Dimitri Gidaspow and M.Syamlal
Department of Chemical Engineering
Illinois Institute of Technology
Chicago, IL 60616

ABSTRACT

A two-dimensional transient computer program developed for fluidization was used to study the uniformity of powders injected into rectangular cavities. Most configurations gave very non-uniform powder distributions. Simulation of a leak present in the experimental bag experiments produced a jet expansion not unlike that observed in photographic records. Simulations with 5, 30 and 200 micron powders showed that the jet expansion was most pronounced with 5-micron powders, and that the powder distribution was the most uniform of the configurations studied.

A comparison of experimental concentration contours obtained from the high-speed photographic records of powder injection showed a reasonably good agreement with the theory. The agreement is considered good, because the theory has no fitted parameters. It is predictive. Discrepancies between the theoretical and experimental results may be qualitatively accounted for by bag expansion and a reduced pressure in the bag due to leaks.

INTRODUCTION

IITRI bag experiments which involve injection of powders into partially-collapsed plastic bags were simulated using a transient two-dimensional two-phase computer program (Gidaspow and Ettehadieh, 1983). The objective was to determine the uniformity of powders for various injection modes. The bags were approximated by a two-dimensional slice with rigid walls. Since the rigid walls may not properly simulate a bag that inflates upon the injection of the powder-air streams, leaky walls were also used in modeling, to give a constant pressure in the two dimensional cavity.

MATHEMATICAL MODEL

The particle injection model uses the principles of conservation of mass and momentum for each phase. It is a two-fluid model of the type reviewed by Lyczkowski, Gidaspow and Solbrig (1982) and by Gidaspow, Rasouli and Shin (1983). Although there are no studies known to the writers dealing with hydrodynamic modeling of powder injections into containers, the modeling dealing with propellant motion by Koo and Kuo (1977) and by Gough (1979) is similar to the present approach. The equations used for powder injection modeling are those developed by Gidaspow and Ettehadieh (1983) for modeling fluidization.

Table I shows the continuity and the separate phase momentum equations for two-dimensional transient two-phase flow. There are six nonlinear coupled partial differential equations for six dependent variables. The variables to be computed are the void fraction, ϵ, the pressure, P, the gas velocity components U_g, V_g, and the solids velocity components U_s and V_s, in the x and y directions, respectively. The equations are written in a form found in the K-FIX computer code (Rivard and Torrey, 1977) for gas-liquid flow.

Table I Hydrodynamic Model

CONTINUITY EQUATIONS

Gas Phase

$$\frac{\partial}{\partial t}(\rho_g\epsilon) + \frac{\partial}{\partial x}(\epsilon\,\rho_g U_g) + \frac{\partial}{\partial y}(\epsilon\,\rho_g V_g) = 0$$

Solid Phase

$$\frac{\partial}{\partial t}[\rho_s(1-\epsilon)] + \frac{\partial}{\partial x}[\rho_s U_s(1-\epsilon)] + \frac{\partial}{\partial y}[\rho_s(1-\epsilon)V_s] = 0$$

MOMENTUM EQUATIONS

Gas Momentum in x Direction

$$\frac{\partial}{\partial t}(\rho_g\,\epsilon\,U_g) + \frac{\partial}{\partial x}(\rho_g\,\epsilon\,U_g U_g) + \frac{\partial}{\partial y}(\rho_g\,\epsilon\,V_g U_g) = -\,\epsilon\,\frac{\partial P}{\partial x} +$$

$$\beta_x(U_s - U_g)$$

Solids Momentum in x Direction

$$\frac{\partial}{\partial t}[\rho_s(1-\epsilon)U_s] + \frac{\partial}{\partial x}[\rho_s(1-\epsilon)U_s U_s] + \frac{\partial}{\partial y}[\rho_s(1-\epsilon)V_s U_s] =$$

$$-(1-\epsilon)\frac{\partial P}{\partial x} + \beta_x(U_g - U_s) - \frac{\partial\tau}{\partial x}$$

Gas Momentum in y Direction

$$\frac{\partial}{\partial t}(\rho_g\,\epsilon\,V_g) + \frac{\partial}{\partial x}(\rho_g\,\epsilon\,U_g V_g) + \frac{\partial}{\partial y}(\rho_g\epsilon\,V_g V_g) =$$

$$-\,\epsilon\,\frac{\partial P}{\partial y} + \beta_y(V_s - V_g) - \rho_g\,\epsilon\,g$$

Solids Momentum in y Direction

$$\frac{\partial}{\partial t}[\rho_s(1-\epsilon)V_s] + \frac{\partial}{\partial x}[\rho_s(1-\epsilon)U_s V_s] + \frac{\partial}{\partial y}[\rho_s(1-\epsilon)V_s V_s] =$$

$$-(1-\epsilon)\frac{\partial P}{\partial y} + \beta_y(V_g - V_s) - \rho_s(1-\epsilon)g - \frac{\partial\tau}{\partial y}$$

Fluid Particle Drag

The major empirical input in this model is the fluid-particle friction co-efficient, β. It is obtained from standard correlations as explained in detail by Gidaspow and Ettehadieh (1983).

For porosities less than 0.8 the pressure drop due to friction between gas and solids can be described by the Ergun equation. The friction coefficient in this porosity range becomes

$$\beta_y = 150 \frac{(1-\varepsilon)^2 \mu_g}{\varepsilon(d_p \phi_s)^2} + 1.75 \frac{\rho_g |V_g - V_s|(1-\varepsilon)}{\phi_s d_p} . \tag{1}$$

For porosities greater than 0.8 Stokes' law corrected for high flow and packing leads to the following expressions for the friction coefficient:

$$\beta_y = \frac{3}{4} C_{Dy} \frac{\varepsilon(1-\varepsilon)|V_g - V_s|\rho_g}{d_p \phi_s} f(\varepsilon), \quad \varepsilon \geq 0.8 \tag{2}$$

where C_{Dy}, the drag coefficient in the y direction, is related to the Reynolds number by means of the well known (Soo, 1967) relations given below.

$$C_{Dy} = \frac{24}{Re_{sy}} (1 + 0.15 \, Re_{sy}^{0.687}), \quad Re_{sy} < 1000 \tag{3}$$

$$C_{Dy} = 0.44 \qquad\qquad Re_{sy} \geq 1000 \tag{4}$$

where

$$Re_{sy} = \frac{\rho_g (V_g - V_s) d_p}{\mu_g} \tag{5}$$

In equation (2) $f(\varepsilon)$ shows the effect due to the presence of other particles in the fluid and acts as a correction to the usual Stokes law for free fall of a single particle. We use

$$f(\varepsilon) = \varepsilon^{-2.65} \tag{6}$$

In the present study this correction is near one and therefore contributes very little to the results. The expression for the friction coefficient in the x direction is the same as that in the axial direction, y.

Solids Stress

In a general formulation the solids momentum equations would contain solids stress terms that are a function of porosity, pressure and the displacement tensors of solids velocity, gas velocity and relative velocity. Such a general formulation with proper values of material constants does not exist today. However, it is necessary to use the normal component of the solids stress to prevent the particles from reaching impossibly low values of void fraction. Measurements of such a stress for settling showed it to be quite small compared with the hydrostatic pressure. In view of the previous theory and measurements, the constitutive equation for the normal component of the stress, τ is

$$\tau = \tau(\varepsilon)$$

Then by chain rule,

$$\frac{\partial \tau}{\partial y} = \frac{\partial \tau}{\partial \varepsilon} \cdot \frac{\partial \varepsilon}{\partial y} \tag{7}$$

Let the modulus of elasticity or particle to particle interaction coefficient be

$$G(\varepsilon) = \frac{\partial \tau}{\partial \varepsilon} \tag{8}$$

In this study this modulus is fitted to the experimental data for fluidization (Gidaspow and Ettehadieh, 1983) by the equation

$$-G(\varepsilon) = 10^{(-8.76\varepsilon + 5.43)}, \text{ N/m}^2 \tag{9}$$

This term becomes of numerical significance only when the void fractions go below the minimum fluidization void fraction. Although this does not happen in this study this term helps to make the system numerically

stable, because it converts the imaginary characteristics into real values.

Fanucci, Ness and Yen (1979) have obtained the characteristic directions for one dimensional incompressible flow for the set of equations shown in Table I. Their paper shows one of their characteristics, C to be

$$C = \left[\frac{1}{\rho_g/\epsilon + \rho_s/\epsilon_s}\right]^{1/2} \left[\frac{-(V_g - V_s)^2}{\epsilon/\rho_g + \epsilon_s/\rho_s} - \frac{G(\epsilon)}{\epsilon_s}\right]^{1/2} \tag{10}$$

The above relation shows that as the void fraction goes to zero $-G(\epsilon)$ becomes large and makes the characteristics real. In practice we find that this extra stress permits us to continue calculations in time without a loss of material balance. Without this term the K-FIX code (Rivard and Torrey, 1977) gave results that showed a loss of mass after about 0.7 seconds of operation even with a very strict convergence criterion.

Boundary and Initial Conditions

Initially there was no powder in the bag. Thus the powder volume fraction is set to zero. The powder of a prescribed volume fraction enters the system at prescribed solid velocities. Since these velocities are high and the inlet gas flow rates are not known, it is assumed that there exists no slip between the powder and the air entering the bag. Thus the gas velocity entering the system is assumed to be equal to the velocity of the fine powder. This assumption may not be exactly correct and may lead to the injection of more air than is true in the IITRI bag experiments. A knowledge of the pressure in the bag before explosion would have been helpful in checking this assumption.

The boundary conditions (B.C.) are as follows (See Figure 1):

B.C.1 At x=0, the prescribed variables are:

At the inlet port, the velocities were constant or as shown below.

$$U_g = U_s = 40 + 10.5 \sin(20\pi t) \qquad t \leq t_o \qquad (11)$$

$$= 0 \qquad\qquad t > t_o$$

where t_o is the time at which the powder flow was terminated.

$$V_g = V_s = 0 \qquad (12)$$

$$\epsilon = 0.998 \qquad (13)$$

Elsewhere at the walls,

$$V_g = V_s = 0 \qquad (14)$$

$$U_g = U_s = 0 \qquad (15)$$

B.C.2

For configurations such as "d" (symmetrical),

At $x = 200$ cm

$$\frac{\partial V_g}{\partial x} = \frac{\partial V_s}{\partial x} = 0 \qquad (16)$$

$$U_g = U_s = 0 \qquad (17)$$

For configurations such as "f",

At $x = 400$ cm

$$V_g = V_s = 0 \qquad (18)$$

$$U_g = U_s = 0 \qquad (19)$$

B.C.3

At $y = 0$

$$V_g = V_s = 0 \qquad (20)$$

$$U_g = U_s = 0 \qquad (21)$$

B.C.4

At $y = 88$ cm

For configurations without any leak,

$$V_g = V_s = 0 \qquad (22)$$

$$U_g = U_s = 0 \tag{23}$$

For configurations with a leak

$$P = \text{atmospheric} \tag{24}$$

$$V_s = 0 \tag{25}$$

Numerics and Computational Time

The two-phase flow equations describing the dynamics of the powder-laden gas were solved using a modified K-FIX program (Rivard and Torrey, 1977). The K-FIX program solves these equations using a semi-implicit technique. The continuity equations are differenced fully implicity, whereas the pressure-term and the drag-term are the only implicit terms in the differenced momentum equations. At any time step these difference equations are solved iteratively, to obtain the updated values of the dependent variables.

The computations were carried out, typically, over a two dimensional region consisting of 150 computational cells. The horizontal direction was discretized into ten parts of 40 cm each and the vertical direction was discretized into 15 parts of a height of 6.1 cm. The simulation of the powder flow inside the bag was typically carried out for two seconds of real time. On a commercial CRAY-I computer, about two minutes of CPU time was expended for each of those computations.

The density plots shown in Figures (2) and (8) are generated from the powder volume fraction data. The number of dots in any computational cell is proportional to the square of the powder volume fraction in that cell. In a visual observation of the actual process such a nonlinear functional relationship between the powder volume fraction and the total projected area is believed to exist.

COMPUTER RESULTS

Figure 1 depicts the various bag configurations for which computer runs were made together with the inlet conditions that were used. Initially the bags contained only air at one atmosphere. Figure 2 shows the powder concentration at various times for configuration "a". The powder moved into the bag with a slug-type motion, was reflected from the wall opposite the inlet and then was returned to the inlet wall. Figure 2 shows that there exists a central void in the cavity containing no powder. This void persisted even after continued injection of powder beyond the 0.8 sec shown in the figure.

Cases b and d' with opposing jets were run by assuming a central symmetry. The computer program was not programmed to handle the non-symmetrical case C, because the computations involve a sweep from one direction. This case would require reprogramming.

EFFECT OF LEAK, SINUSOIDAL INPUT AND MIXING

The introductory runs had shown the powder motion to be of an almost slug type. It was suspected that this was in part due to the build up of pressure in the cavity which prevented a large lateral particle motion. For example, for configuration d the pressure rose to 4.8 atmospheres after 0.7 seconds of powder injection. In the IITRI bag experiment the pressure is clearly not that high because of bag expansion and leaks. To simulate this situation properly a leak along the upper boundary was allowed in configuration "e". The leak was such that the pressure in the bag stayed at essentially one atmosphere.

To further correct for greater jet expansion in the lateral direction, a sinusoidal variation of the inlet velocity was taken. Figures 3a and 3b show that the sinusoidal variation had a negligible effect on the

jet expansion. However, a comparison of Figures 3a and 3b to Figures 3c and 3d shows that the leak had a very large effect on the lateral jet expansion. Nevertheless, the run with the leak shows that the powder continued to move horizontally as well as vertically in the direction of the leak; a more complex behavior was obtained due to the lack of restraining pressure that had been present in the runs with no leaks.

Figure 4 shows the gas velocities for configuration d, with no leak. The gas flow reaches an almost steady circulatory motion after about 0.1 seconds of powder injection. The solid, on the other hand, lags considerably behind the gas motion; as indicated previously in Figure , at 0.2 seconds there was no solid present along the top and bottom w . Figure 5 shows the gas velocities with a leak for configuration e. e gas velocities on the top face are considerably modified by the leak in the expected manner, that is, flowing out of the cavity. The solid partially moved up, but did not follow the gas stream lines.

Figure 6 shows the concentration profiles with and without leak at 0.1 seconds at various positions in the cavity. Generally, the solid moved toward the leak, but there exists a wave motion. For example, in Figure 6b the solid moved away from the leak and tended to accumulate near the boundary opposite the leak. Figure 7 shows the concentration profiles after 0.2 seconds of powder injection. The accumulation of solids is more pronounced due to the wave motion.

In runs "d" to "f" the powder was terminated at 0.82 seconds and at 0.53 seconds, but the powder was allowed to mix due to inertia of the particles rotating in the cavity. An examination of the computer output of solids volume fractions showed that a great uniformity of particles was produced by this mode of operation. However, there was

a considerable settling and accumulation of powder at the bottom of the cavity. See Table II.

PARTICLE SIZE EFFECT

The effect of particle size was studied in configurations "g" to "i". Figure 8 shows the particle concentrations at 0.1 and 0.2 seconds for particle sizes of 5, 30 and 200 microns. Even with the leak, the 200-micron particles moved in a slug-type fashion, as shown in Figures 8e and 8f. Figure 8d shows that the five-micron powder filled the complete bag as early as 0.2 seconds. No voids were present at this time in the computation, in contrast to that for the standard 30-micron powder.

POWDER UNIFORMITY

A computer run was made for configuration j, with two opposing jets at the top and for the standard 30-micron powder. Table III shows the uniformity that can be achieved with this size powder by utilizing such a configuration.

COMPARISON TO HIGH-SPEED PHOTOGRAPHIC RECORDS

A comparison of the computed profiles to those observed in high-speed photographs was made (See Figure 9). The dashed curves are the contours of a solid volume fraction of $2x10^{-4}$. This is ten percent of the incoming volume fraction of the solids. At a time up to 0.040 seconds these computed contours agreed with the contours obtained from the movies of the experiment. At later times this computed powder concentration reached the far end of the bag earlier than shown in the experimental photographic records. This may be due to the fact that in the experiment the bag was partially deflated initially, thus offering resistance to the forward flow of powder. After powder deflection from the end of the bag, experimental and theoretical results again are in agreement. For example, the

shape of the computed jet closely resembled the observed jet shape. The theoretical computations and the experimental results both showed a narrowing and a widening of the jet.

Figure 9 also shows the computed concentration profiels for a volume fraction of the solid equal to 18×10^{-4} at 0.040 and 0.070 seconds. This is 90 percent of the inlet volume fraction. This concentration lags considerably behind the 10 percent of inlet volume fraction. Clearly, the dispersion of the powder is quite large. Hence a better correlation of theoretical and experimental results would require a knowledge of the value of powder concentration at the visible concentration front. It is possible that the computations could provide an estimate of the solid volume fraction visible in high speed photographic records. In addition, discrepancies concerning the initial shape of the bag and the amount and location of leaking exist between the computer modeling and the experimental work. As these discrepancies are resolved better agreement between the theory and experiment should be obtained.

REFERENCES

Fanucci, J.B., Ness N. and Yen R.H., "On the Formation of Bubbles in Gas-Particulate Fluidized Beds," J. Fluid Mech., Vol. 94, part 2, pp. 353-367 (1979).

Gough, P.S., "Two-Dimensional Convective Flame-Spreading in Packed Beds of Granular Propellent," ARBAL-CR-00404, July 1979 to Ballistic Research Laboratory, Aberdeen Proving Ground, Maryland.

Gidaspow, D. and Ettehadieh, B. "Fluidization in Two Dimensional Beds with a Jet. Part II. Hydrodynamic Modeling," I&EC Fundamentals, 22, 193-201 May (1983).

Gidaspow, D., Rasouli, F. and Shin, Y.W. "An Unequal Velocity Model for Transient Two-Phase Flow by the Method of Characteristics" Nuclear Science and Engineering 84, 179-195 (1983).

Koo, J.H. and Kuo, K.K., "Transient Combustion in Granular Propellant Beds; Part I: Theoretical Modeling and Numerical Solution of Transient Combustion Processes in Mobile Granular Propellant Beds," Final Report February 15, 1974-February 14, 1977, BRL-CR-346, Ballistic Research Laboratory, AD-A044998, Aberdeen Proving Ground, Aberdeen, Maryland (Aug. 1977).

Lyczkowski, R.W., Gidaspow, L. and Solbrig, C.W., "Multiphase Flow-Models for Nuclear, Fossil and Biomass Energy Conversion", Chapter in Vol. II of Advances in Transport Processes, A.S. Majumdar and R.A. Mashelkar, Editors, Wiley-Eastern Publisher, pp 198-351, 1982.

Rivard, W.C. and Torrey, M.D., "K-FIX: A Computer Program for Transient, Two-Dimensional, Two Fluid Flow" Los Alamos, LA-NUREG-6623 (1977).

Soo, S.L., "Fluid Dynamics of Multiphase Systems", Blaisdell Publishing Co., Waltham, MA (1967).

NOTATION

C_D	Drag coefficient
d_p	Diameter of solid particles, m
g	Gravitational force per unit mass, m/sec^2
G	Modulus of elasticity, particle-particle interaction coefficient, N/m^2
P	Pressure, Pa
Re_s	Solids Reynolds number
t	Time, sec.
U_g	Lateral gas velocity, m/sec
U_s	Lateral solid velocity, m/sec
V_g	Axial gas velocity, m/sec.
V_s	Axial solid velocity, m/sec.
x	Co-ordinate in lateral direction, m
y	Co-ordinate in axial direction, m

Greek Letters

β_x and β_y	Fluid-particle friction coefficient in the x and y directions K_g/m^3-sec.
ϵ	Gas volume fraction
τ	Solids stress, related to particle-particle pressure, N/m^2.
μ_g	Gas viscosity, Kg/(m.sec)
ρ_g	Gas density, Kg/m^3
ρ_s, ρ_p	Solid and particle densities, Kg/m^3
ϕ_s	Sphericity

0.1118E-01	0.5794E-02	0.6351E-02	0.7255E-02	0.8591E-02
0.1168E-01	0.3522E-02	0.2755E-02	0.2466E-02	0.4854E-02
0.1029E-01	0.1935E-02	0.3151E-03	0.7124E-03	0.3705E-02
0.8317E-02	0.0000	0.0000	0.0000	0.3367E-02
0.7061E-02	0.1421E-13	0.2781E-05	0.7574E-05	0.3066E-02
0.6195E-02	0.1808E-03	0.5344E-03	0.1436E-03	0.2888E-02
0.5573E-02	0.4865E-03	0.6767E-03	0.1495E-03	0.2605E-02
0.5059E-02	0.7852E-03	0.6833E-03	0.1903E-03	0.2101E-02
0.4649E-02	0.1217E-02	0.5425E-03	0.2648E-03	0.3327E-02
0.4273E-02	0.8900E-03	0.3108E-03	0.4161E-03	0.5000E-02
0.3970E-02	0.1244E-02	0.7861E-03	0.2766E-03	0.6399E-02
0.3689E-02	0.1584E-02	0.1827E-02	0.1524E-02	0.7763E-02
0.3647E-02	0.1671E-02	0.1395E-02	0.0000	0.8532E-02
0.1052E-01	0.4346E-02	0.1224E-03	0.1944E-03	0.1177E-01
0.3838	0.5560E-01	0.3826E-01	0.4372E-01	0.7682E-01

0.4474E-02	0.2474E-02	0.2543E-02	0.2920E-02	0.3385E-02
0.6669E-02	0.2672E-02	0.2726E-02	0.3425E-02	0.5049E-02
0.7646E-02	0.2554E-02	0.2524E-02	0.2400E-02	0.3739E-02
0.7664E-02	0.2364E-02	0.4903E-03	0.9052E-04	0.3050E-02
0.6684E-02	0.4258E-03	0.2781E-05	0.5495E-05	0.2456E-02
0.6155E-02	0.1007E-03	0.5344E-03	0.5635E-04	0.2065E-02
0.5656E-02	0.3303E-03	0.6767E-03	0.5774E-04	0.1815E-02
0.5264E-02	0.6260E-03	0.6533E-03	0.1466E-03	0.1565E-02
0.5001E-02	0.9017E-03	0.5425E-03	0.1692E-03	0.1882E-02
0.4726E-02	0.1340E-02	0.3108E-03	0.2863E-03	0.2535E-02
0.4501E-02	0.9591E-03	0.5717E-03	0.2136E-03	0.3355E-02
0.4330E-02	0.1053E-02	0.7556E-03	0.1242E-02	0.4322E-02
0.5040E-02	0.1586E-02	0.1509E-02	0.0000	0.5240E-02
0.1558E-01	0.4376E-02	0.1470E-02	0.4331E-03	0.7895E-02
0.4263	0.5536E-01	0.3784E-01	0.4303E-01	0.7241E-01

Table II. Solid volume fractions for configuration "d" after
1.1 seconds (top table) and 1.2 seconds (bottom table)
(The tables show the values at the left half of the
cavity at 40cm intervals horizontally and 6.1cm
intervals vertically)

```
0.3579E-01   0.6146E-01   0.6922E-01   0.7245E-01   0.1663
0.1671E-01   0.2179E-01   0.1934E-01   0.1788E-01   0.1315
0.1955E-01   0.2371E-01   0.1849E-01   0.1695E-01   0.1137
0.2279E-01   0.2579E-01   0.1680E-01   0.1593E-01   0.9925E-01
0.3149E-01   0.2660E-01   0.1375E-01   0.1448E-01   0.8974E-01
0.4582E-01   0.2384E-01   0.1149E-01   0.1335E-01   0.8215E-01
0.4512E-01   0.2262E-01   0.1225E-01   0.1300E-01   0.7931E-01
0.4542E-01   0.2251E-01   0.1445E-01   0.1289E-01   0.7923E-01
0.4811E-01   0.2583E-01   0.1725E-01   0.1455E-01   0.8147E-01
0.4756E-01   0.2906E-01   0.2156E-01   0.2019E-01   0.8424E-01
0.5001E-01   0.3334E-01   0.2616E-01   0.3004E-01   0.8455E-01
0.5409E-01   0.3876E-01   0.3637E-01   0.4170E-01   0.8261E-01
0.5615E-01   0.4544E-01   0.4532E-01   0.5276E-01   0.7964E-01
0.6569E-01   0.5331E-01   0.5482E-01   0.6216E-01   0.7951E-01
0.7461E-01   0.6482E-01   0.6750E-01   0.7526E-01   0.8199E-01
```

```
0.1275       0.1251       0.1111       0.7857E-01   0.6663E-01
0.4250E-01   0.3475E-01   0.2971E-01   0.2523E-01   0.7036E-01
0.4364E-01   0.3419E-01   0.2457E-01   0.2410E-01   0.6334E-01
0.4627E-01   0.3429E-01   0.2358E-01   0.2222E-01   0.6335E-01
0.4898E-01   0.3454E-01   0.2425E-01   0.2259E-01   0.5763E-01
0.5152E-01   0.3531E-01   0.2518E-01   0.2364E-01   0.7349E-01
0.5415E-01   0.3707E-01   0.2655E-01   0.2452E-01   0.7873E-01
0.5661E-01   0.4015E-01   0.2581E-01   0.2520E-01   0.7751E-01
0.5676E-01   0.4475E-01   0.2686E-01   0.2699E-01   0.7957E-01
0.6042E-01   0.5009E-01   0.3295E-01   0.3128E-01   0.8343E-01
0.6185E-01   0.5761E-01   0.3403E-01   0.3695E-01   0.8781E-01
0.6338E-01   0.5545E-01   0.4551E-01   0.4414E-01   0.9183E-01
0.6562E-01   0.6853E-01   0.4434E-01   0.5084E-01   0.9509E-01
0.7179E-01   0.7499E-01   0.5723E-01   0.5735E-01   0.9654E-01
0.8159E-01   0.7815E-01   0.6259E-01   0.7240E-01   0.9397E-01
```

Table III. Solid volume fractions for configuration "J" after 0.7 seconds (top table) and 1.0 second (bottom table) (The tables show the values at the left half of the cavity at 40 cm intervals horizontally and 6.1 cm intervals vertically).
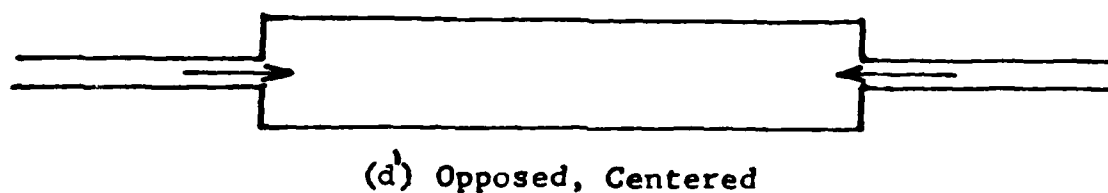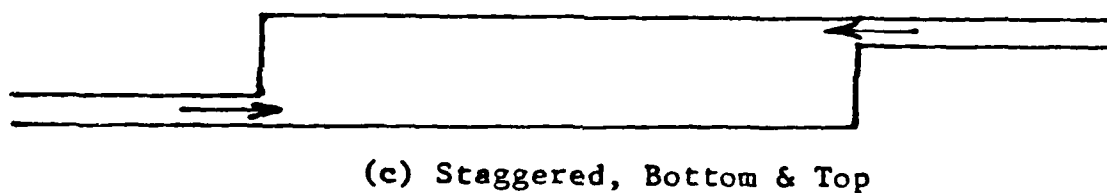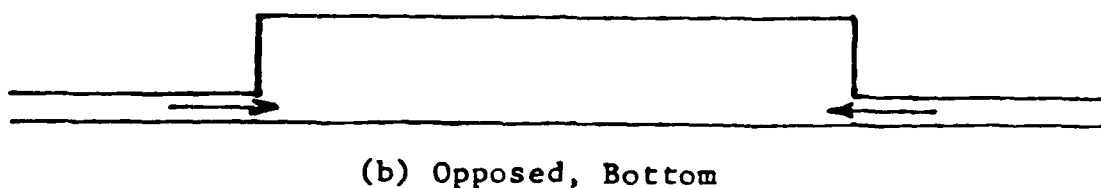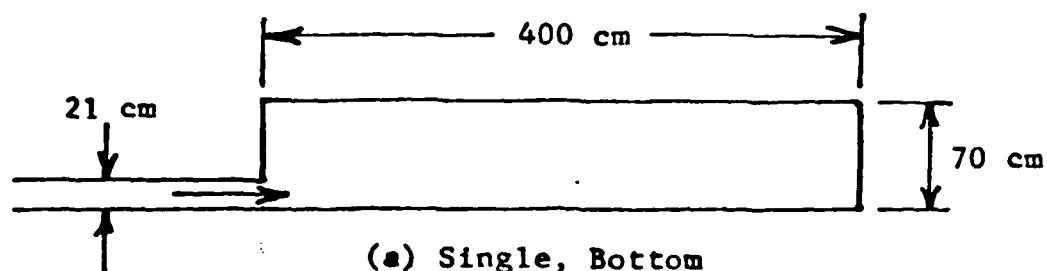
Figure 1A   Four Bag Dissemination Configurations
(Gas velocity = 40 m/sec; Particle
diameter = 30μm, particle density = 1.65 gm/cc;
Inlet solids volume fraction = 0.002).

30.5 cm

400 cm

88 cm

Terminate powder at 0.82 sec
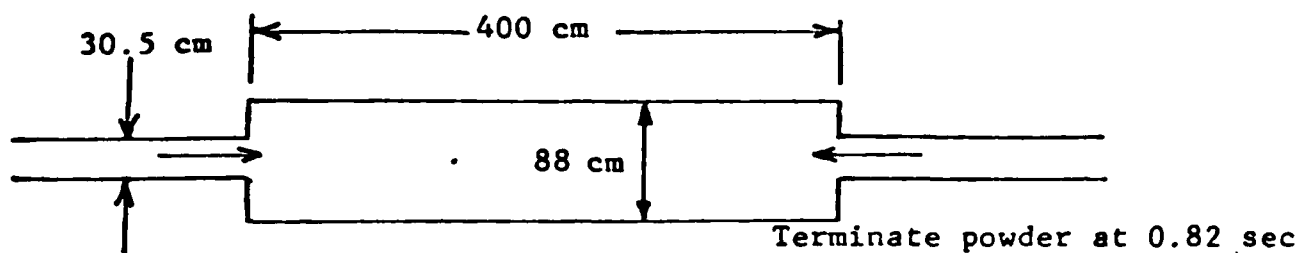
(d) Opposed, Centered, ~~No~~
No Leak

30.5 cm

Leak

88 cm

Terminate powder at 0.82 sec
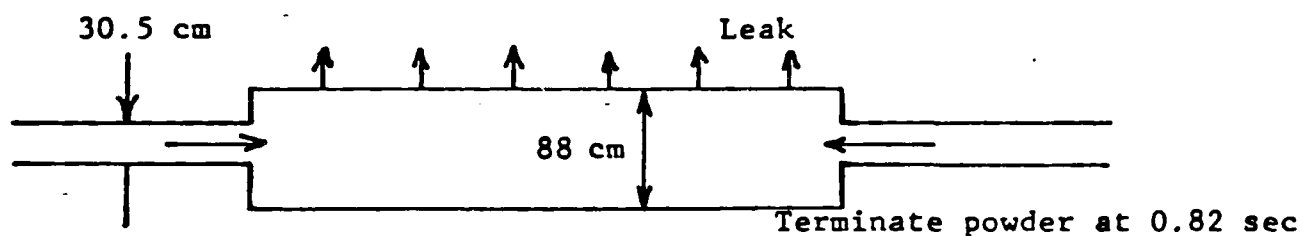
(e) Opposed, Centered,
Uniform Leak across Top

30.5 cm

Leak

88 cm

Terminate powder at 0.53 sec
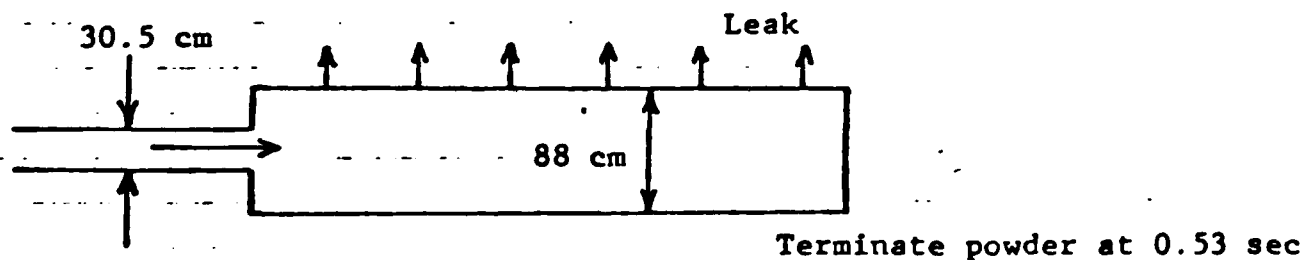
(f) Centered, Single,
Uniform Leak across Top

Figure 1B   Three Bag Dissemination Configurations
(Sinusoidal gas inlet velocity (m/sec) =
40 + 10.5 Sin(20πt), where t is in seconds;
particle diameter = 30μm; particle
density = 1.65 gm/cc; Inlet solids volume
fraction = 0.002)

Powder Termination Time, sec	Powder Particle Size, um
0.53	30
0.53	5
0.53	200

(g)

(h)

(i)

Leak

88 cm

400 cm

30.5 cm

12.2 cm
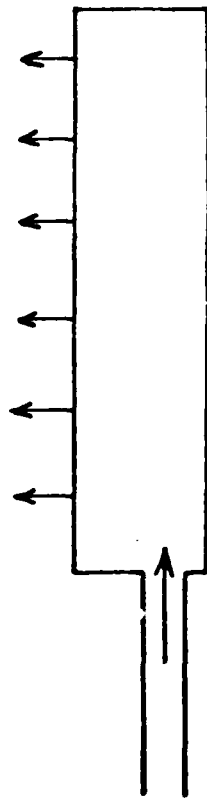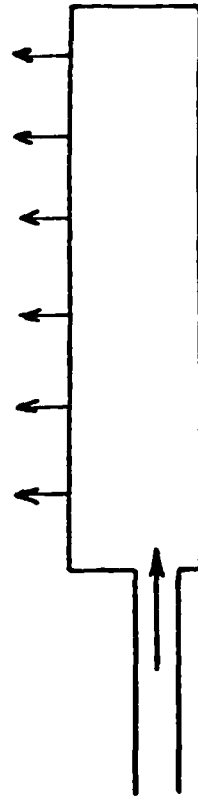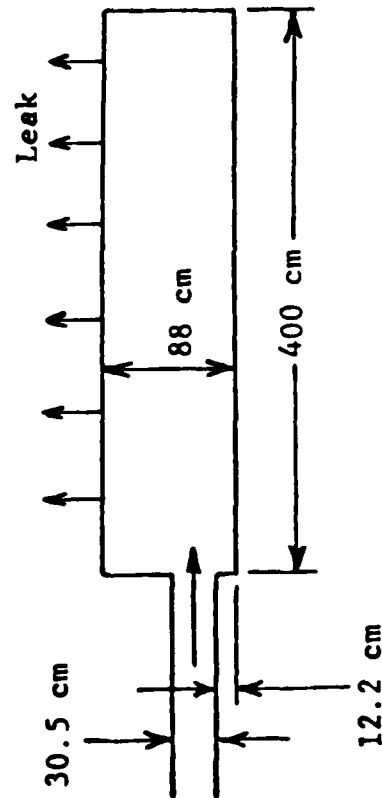
Figure 1C Three Bag Dissemination Configurations with Offset Single Source, and Uniform Leak as Shown (Sinusoidal gas inlet velocity (m/sec) = $40 + 10.5 \sin(20\pi t)$; particle density = 1.65 gm/cc; Inlet solids volume fraction = 0.001)

(j)
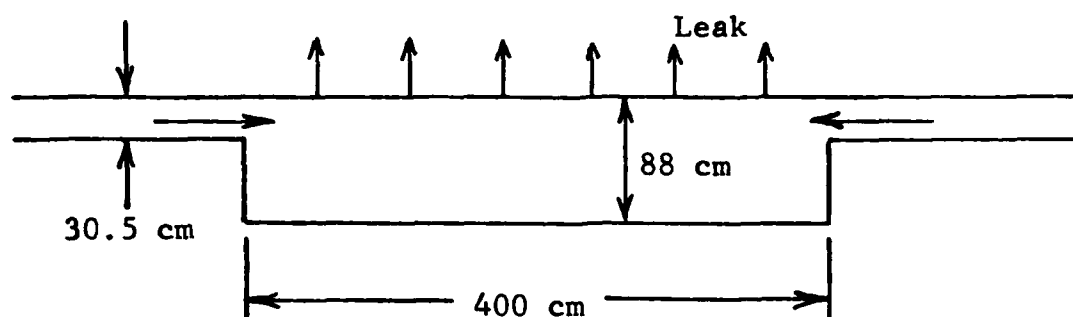
Powder Termination Time = 0.82 sec

Powder Particle Size = 30 μm

Inlet Void Fraction = 0.999

v = 40m/sec

Sinusoidal gas inlet

Velocity (m/sec) = 40 $\pm$ 10.5 Sin(20πt)
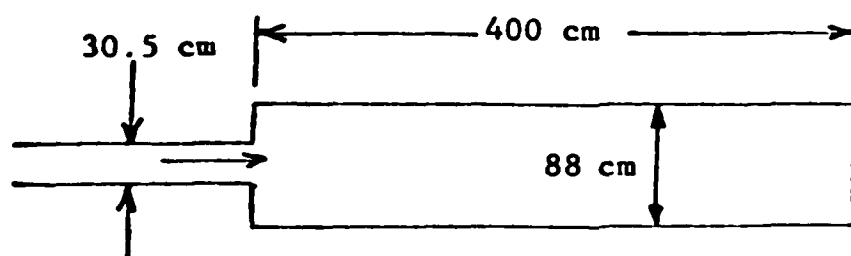
(k) Opposed, Centered,
No Leak

Figure 1D Bag Dissemination Configuration with Opposed Sources
at Top, and Uniform Leak as Shown (top figure)
and Single Source, No Leak(bottom figure).
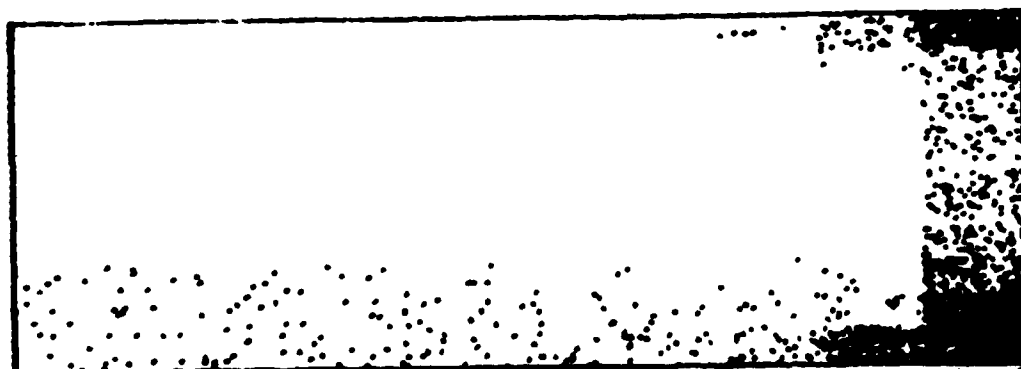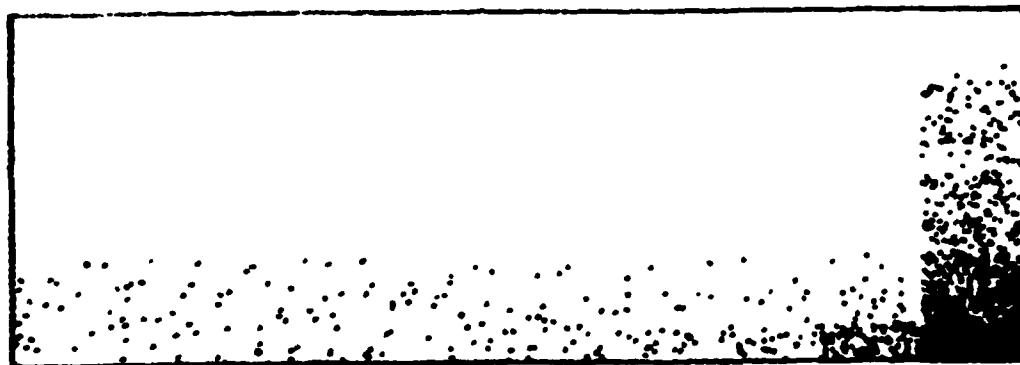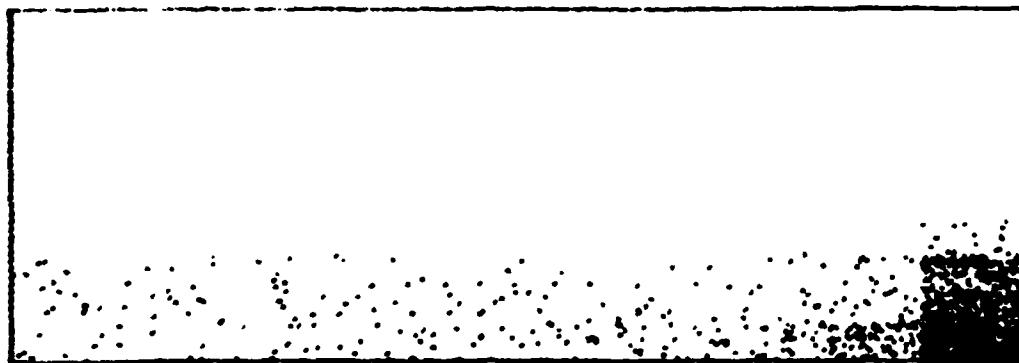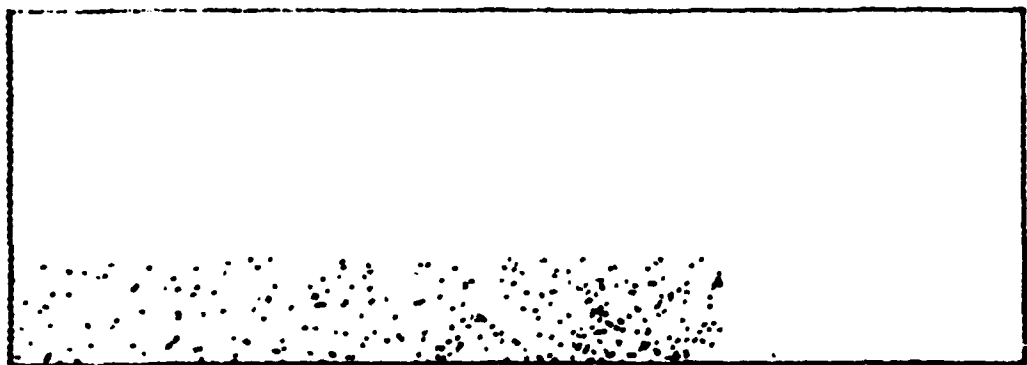
Figure 2A Powder concentration at 0.1, 0.2, 0.3 and 0.4 seconds after
injection. Single inlet, injection velocity 40m/sec,powder
volume fraction 0.002; 70 cm vertical dimension, 400 cm
horizontal; inlet entrance 21 cm.
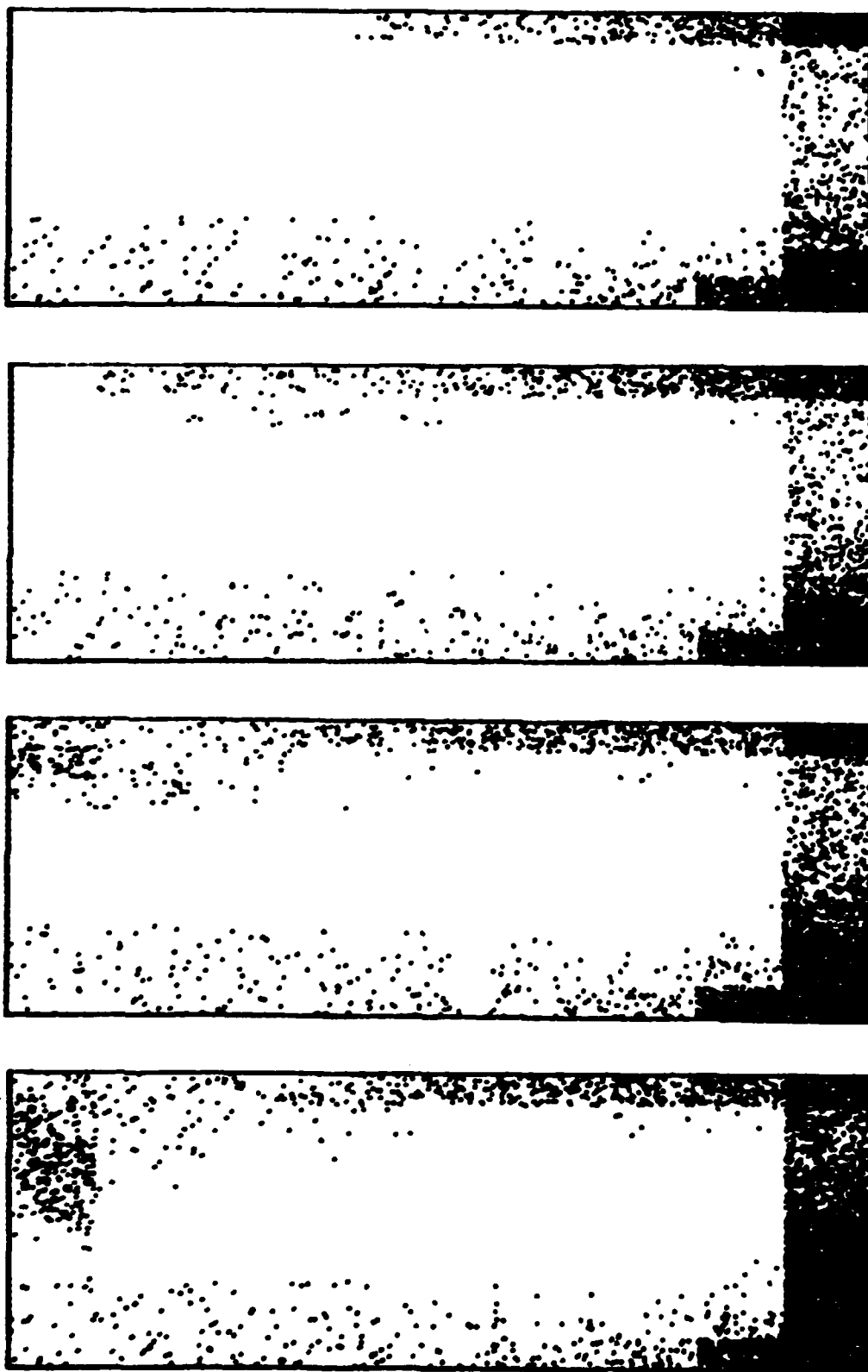
Figure 2B. Powder concentration at 0.5, 0.6, 0.7 and 0.8 sec.
Continuation of Fig.2A.
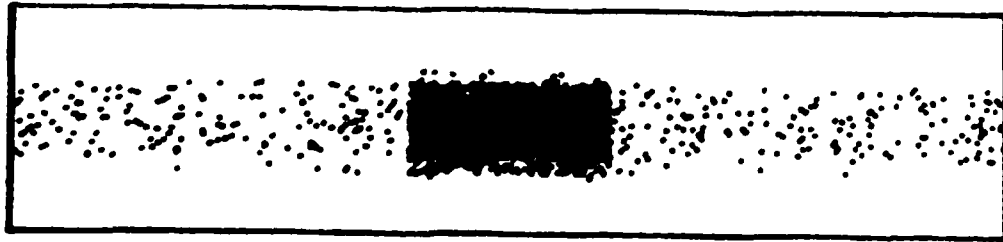
Fig. 3a. Powder concentrations with no leak at 0.1 sec.
Configuration d.
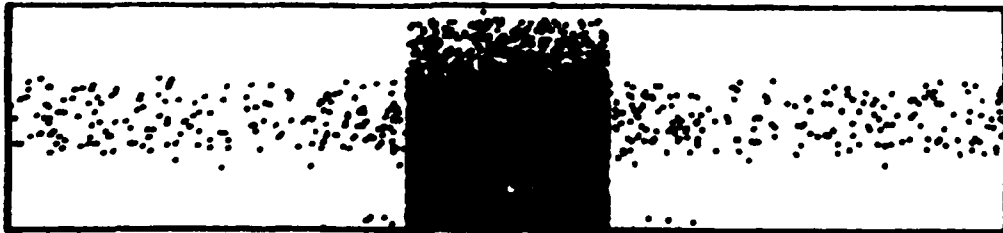
Fig. 3b. Powder concentrations with no leak at 0.2 sec.
Configuration d.
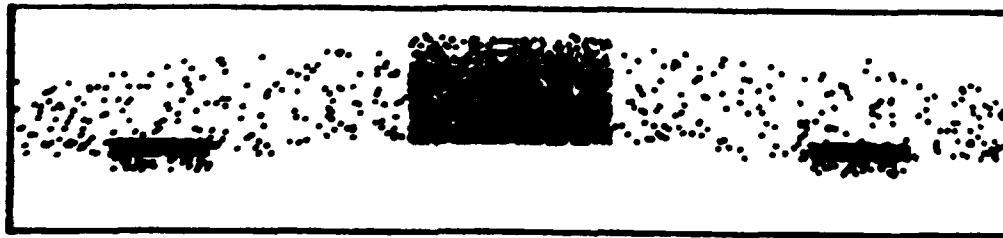
Fig. 3c. Powder concentrations with a leak on top surface
at 0.1 sec. Configuration e.

Fig. 3d. Powder concentrations with a leak on top surface
at 0.2 sec. Configuration e.

Figure 3. EFFECT OF LEAK ON POWDER VOLUME FRACTIONS FOR
INJECTION WITH TWO OPPOSING JETS.
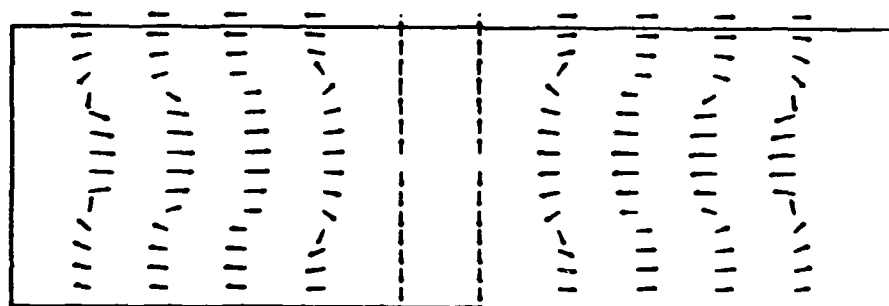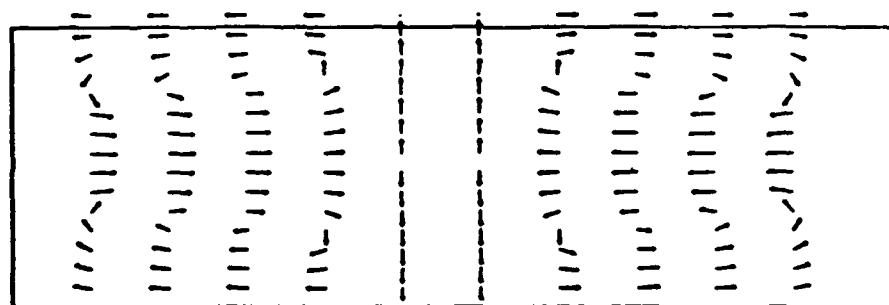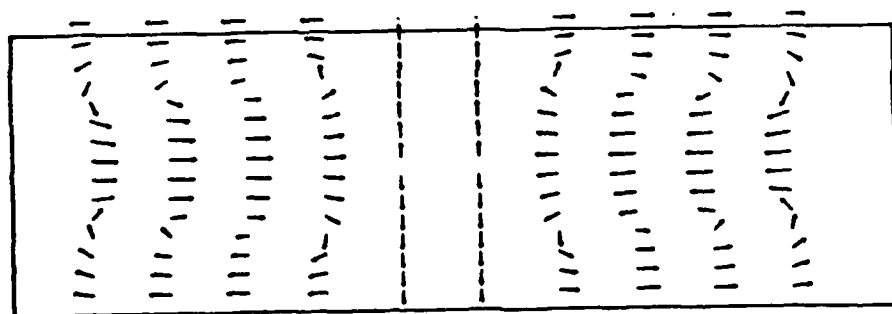
Fig. 4. Gas Velocities for configuration d with no
leak at 0.1, (top graph), 0.2 (middle graph)
and at 0.3 seconds (bottom graph)
Scale: 1 cm = 107 m/sec.
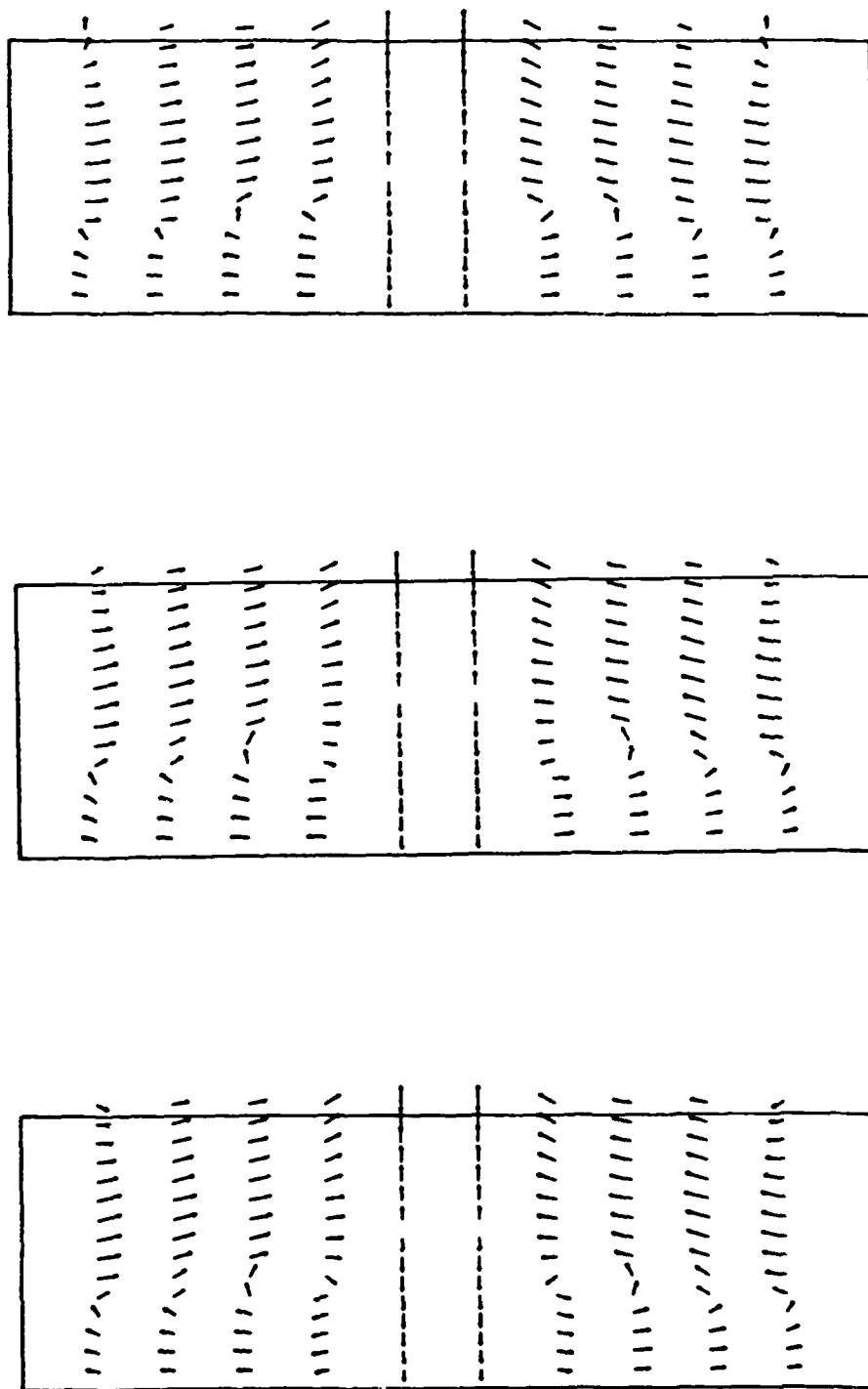
Fig. 5. Gas Velocities for configuration (e) with a leak at 0.1 (top graph), 0.2 (middle graph) and at 0.3 seconds (bottom graph). Scale: 1 cm = 107 m/sec.
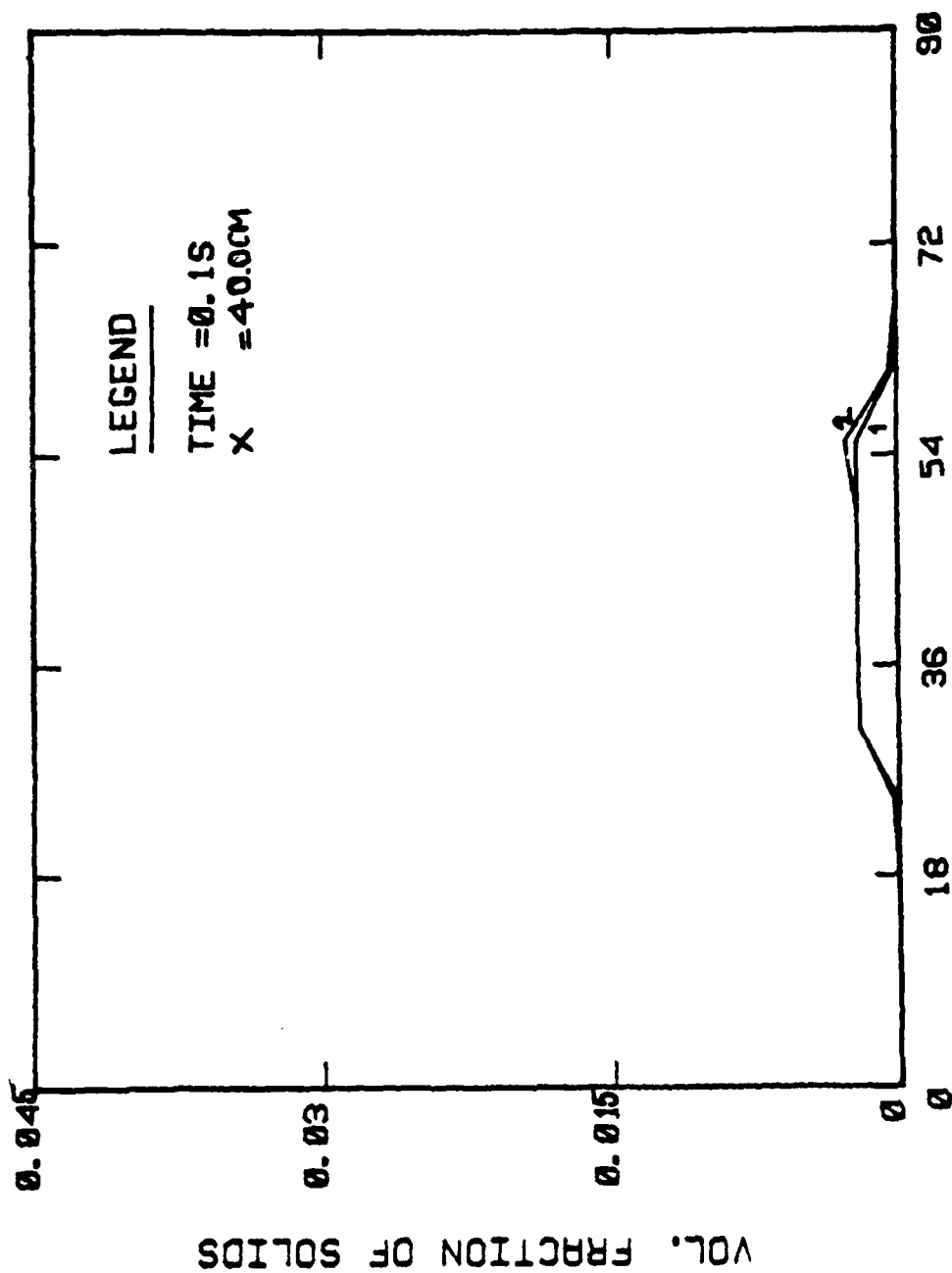
Fig. 6a. Effect of Leak on Powder Concentration at 0.1 seconds at Various positions. Legend: 1 - no leak, configuration d. 2-with leak, configuration e.
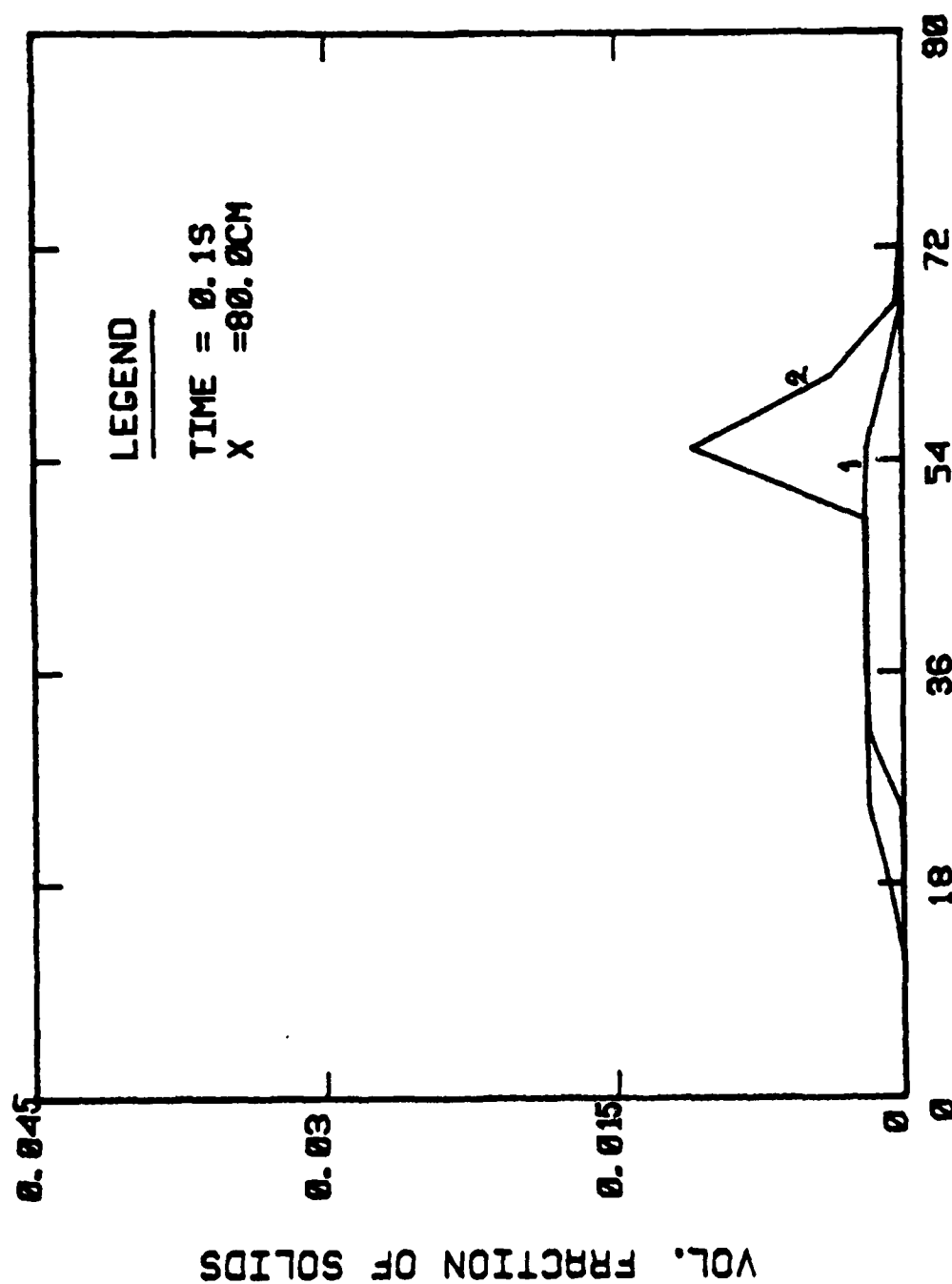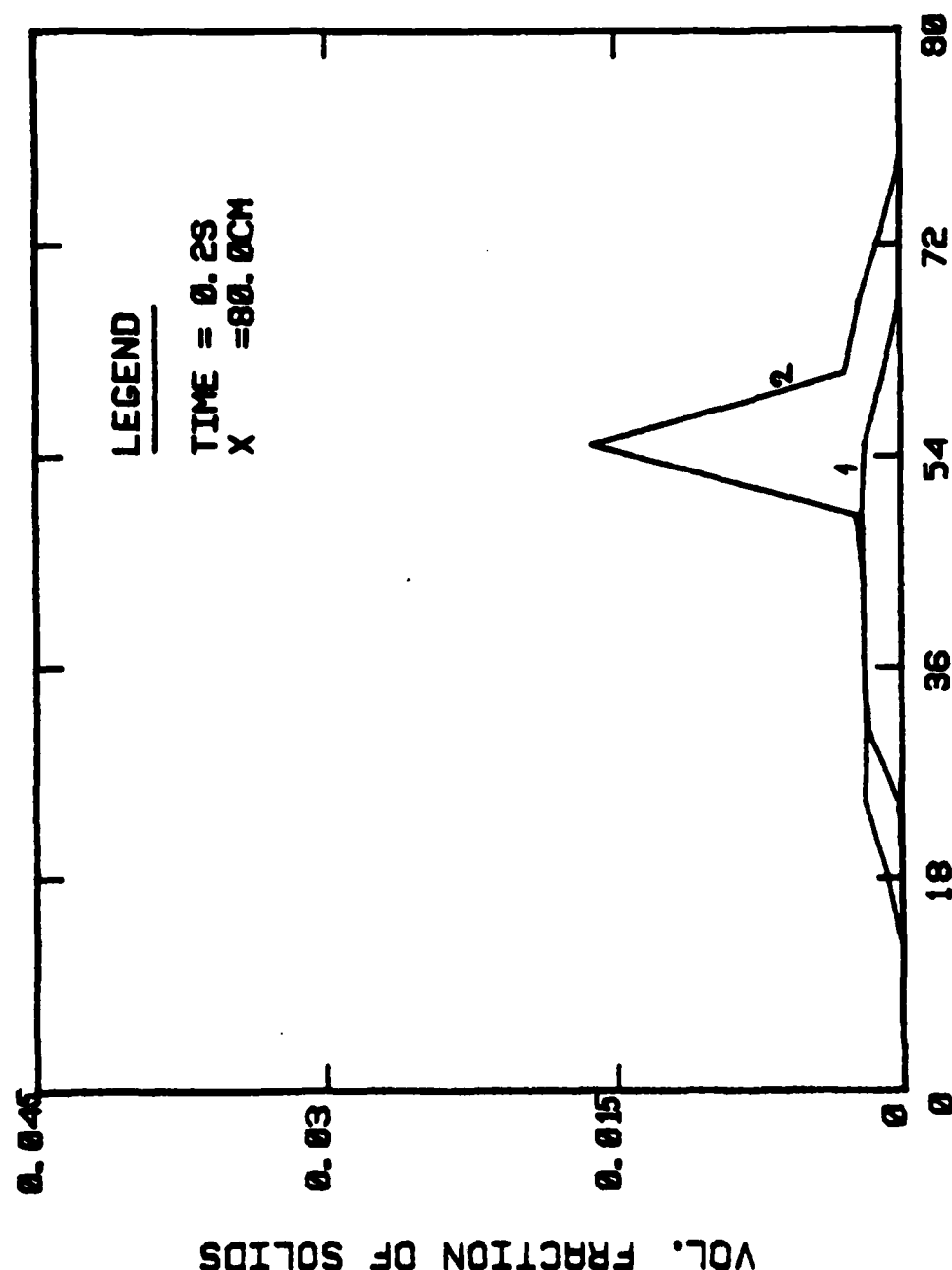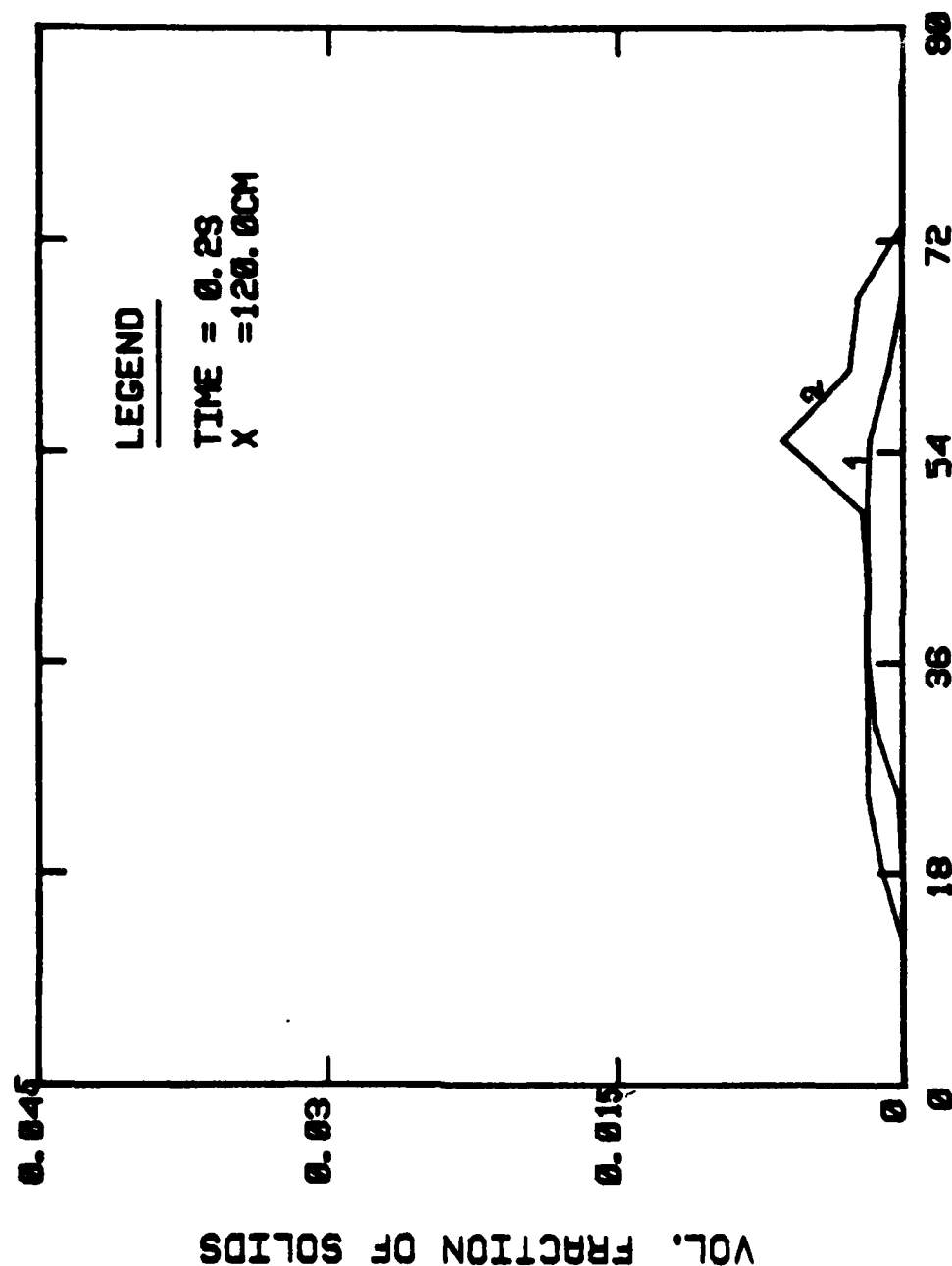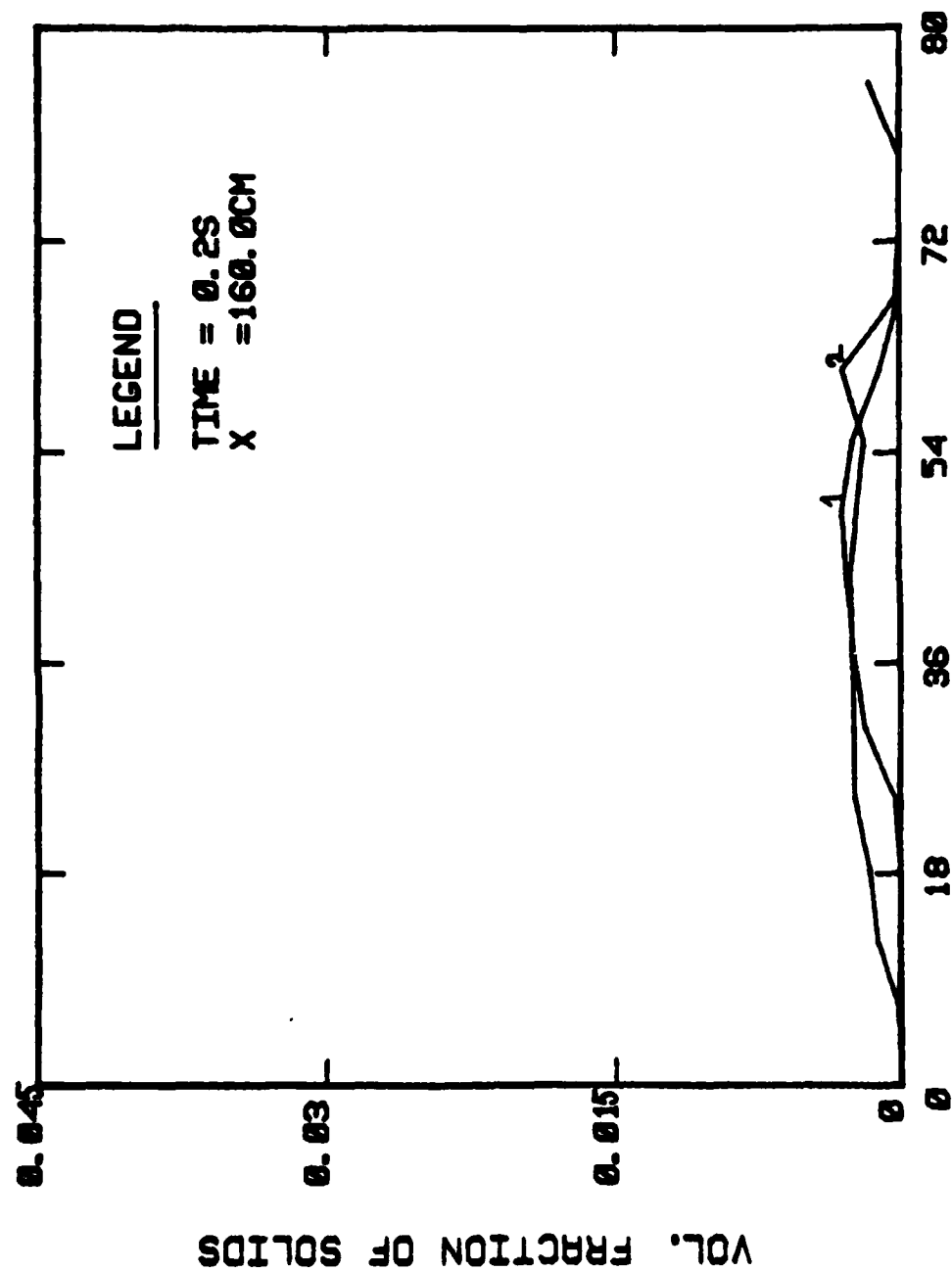
Fig. 6b. Effect of Leak on Powder Concentration at 0.1 seconds at Various Positions. Legend: 1-no leak. configuration d. 2 - with leak, configuration e.
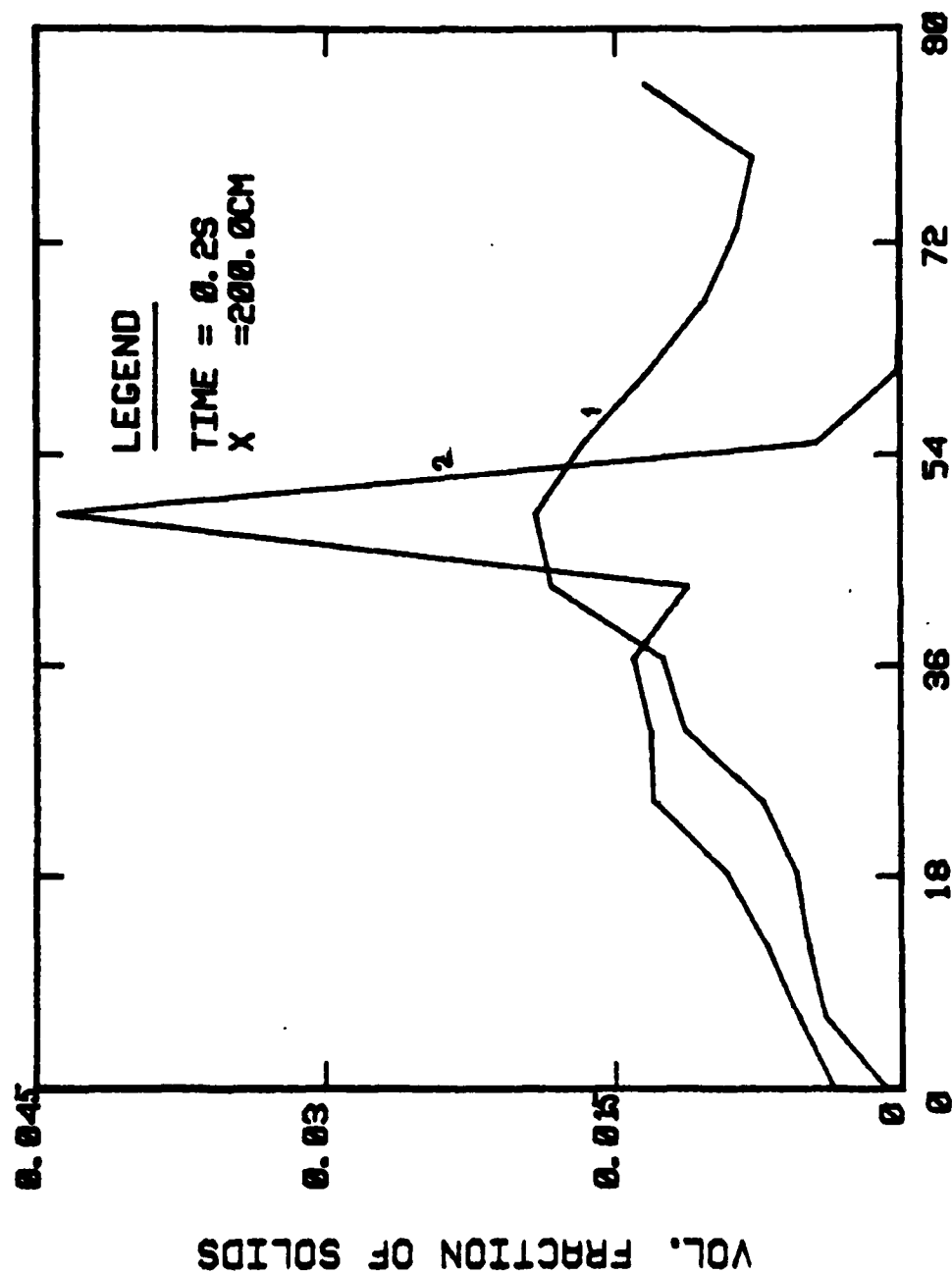
Fig. 6c. Effect of Leak on Powder Concentration at 0.1 seconds
at Various Positions. Legend: 1-no leak, configura-
tion d. 2-with leak, configuration e.

LEGEND

TIME = 0.1S
X =160.0CM

DIST. FROM THE TOP

VOL. FRACTION OF SOLIDS
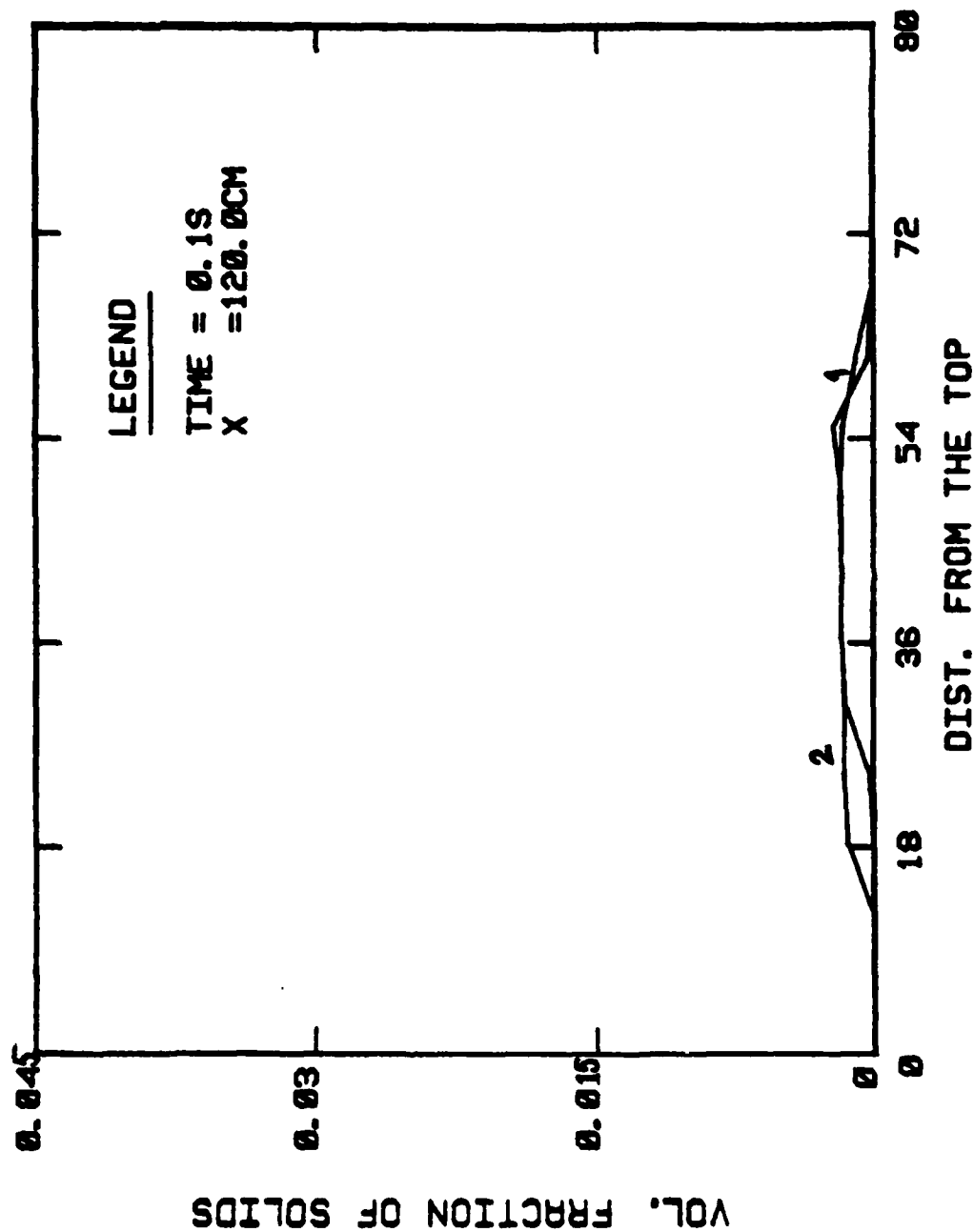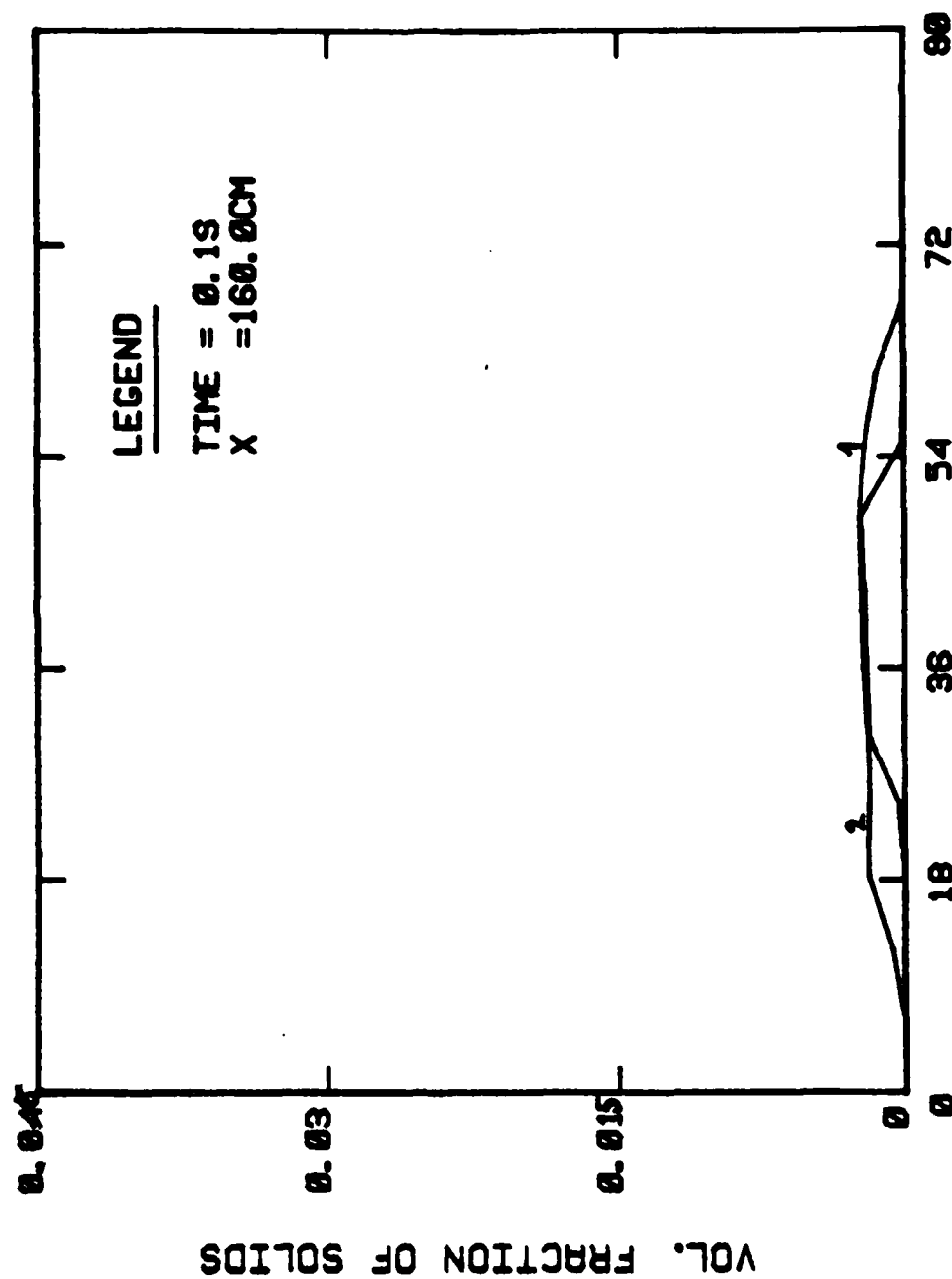
Fig. 6d. Effect of Leak on Powder Concentration at 0.1 seconds at Various Positions. Legend: 1-no leak, configuration d. 2-with leak, configuration e.
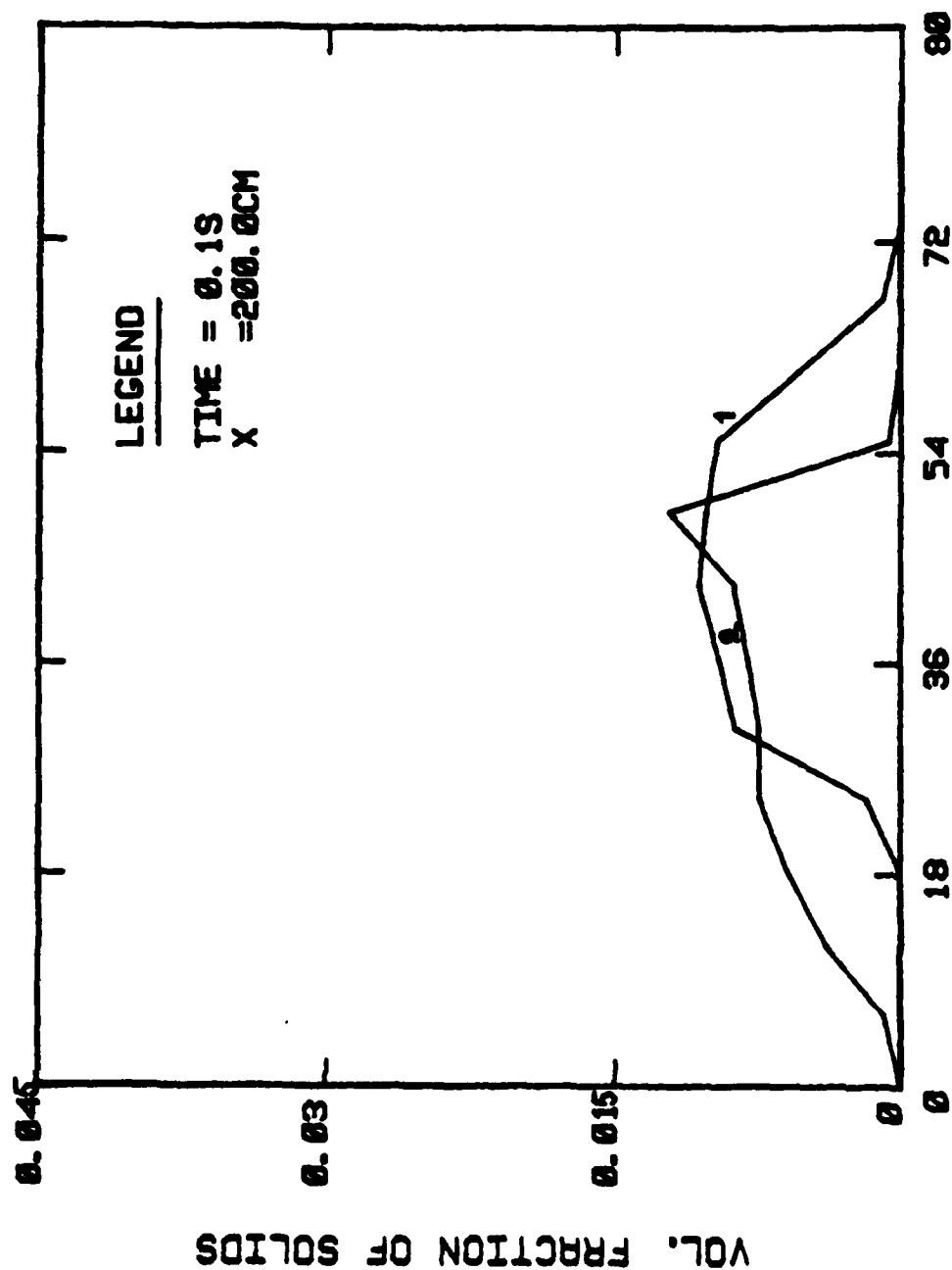
Fig. 6e. Effect of Leak on Powder Concentration at 0.1 seconds at Various Positions. Legend: 1-no leak, configuration d. 2-with leak, configuration e.

Fig. 7a. Effect of Leak on Powder Concentration at 0.2 seconds
at Various Positons. Legend: 1-no leak, configuration d.
2-with leak, configuration e.

VOL. FRACTION OF SOLIDS

0.045

0.03

0.015

0

0 18 36 54 72 80

DIST. FROM THE TOP

LEGEND

TIME = 0.2S
X =80.0CM

2

1
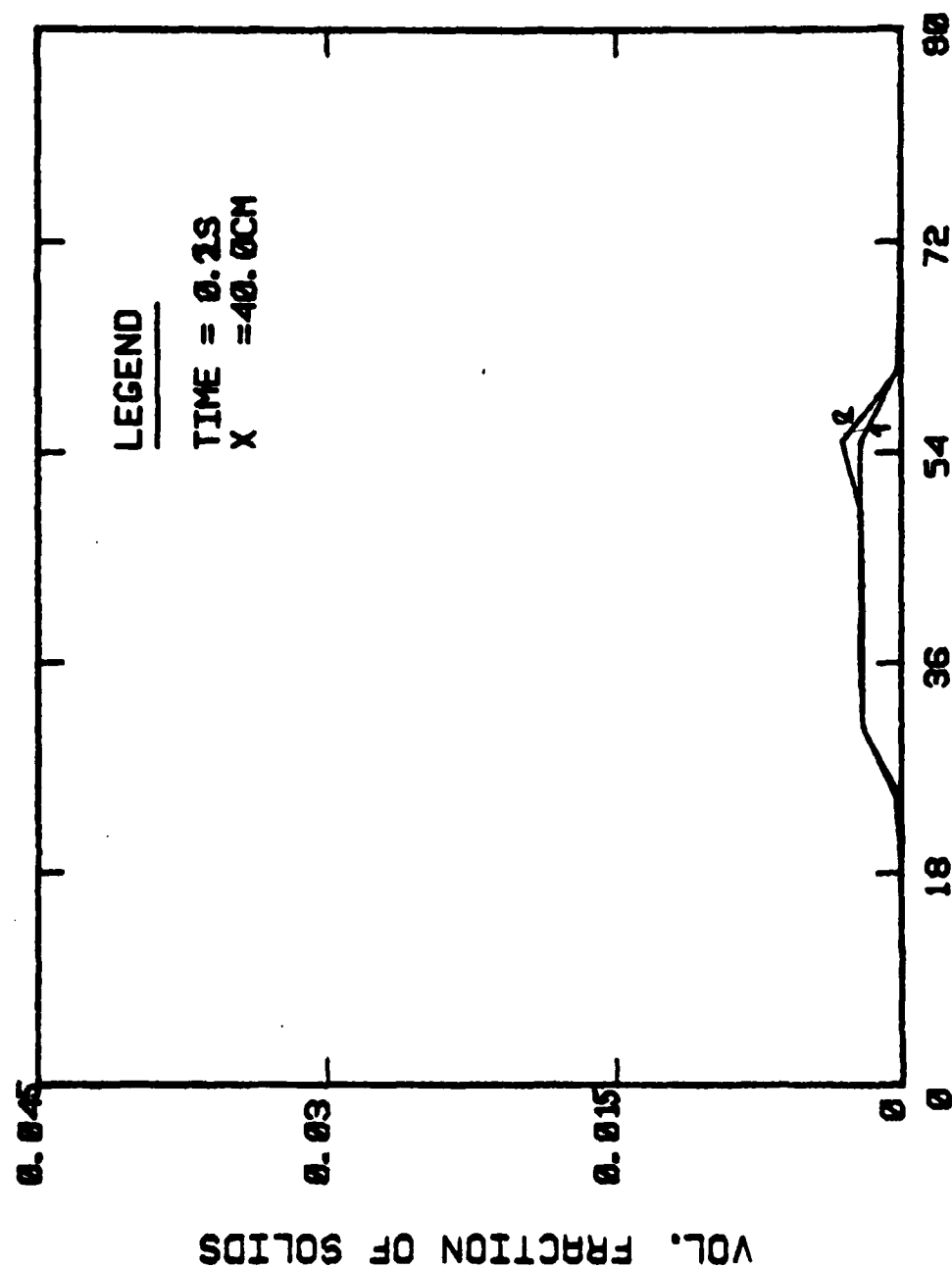
Fig. 7b. Effect of Leak on Powder Concentration at 0.2 seconds
at Various Positions. Legend: 1-no leak, configuration d.
2-with leak, configuration e.

Fig. 7c. Effect of Leak on Powder Concentration at 0.2 seconds at Various Positions. Legend: 1-no leak, configuration d. 2-with leak, configuration e.

Fig. 7d. Effect of Leak on Powder Concentration at 0.2 seconds at Various Positions. Legend: 1-no leak, configuration d. 2-with leak, configuration e.

34

Fig. 7e. Effect of Leak on Powder Concentration at 0.2 seconds at Various Positions. Legend: 1-no leak, configuration d. 2-with leak, configuration e.

Fig. 8a. Powder concentrations for 30 µm particles at 0.1 sec. Configuration g.

Fig. 8b. Powder concentrations for 30 µm particles at 0.2 sec. Configuration g.
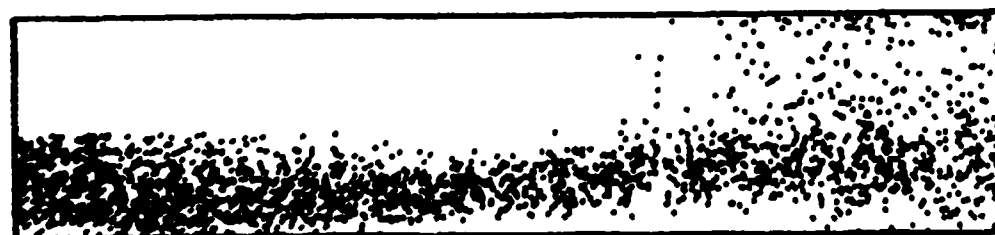
Fig. 8c. Powder concentrations for 5 µm particles at 0.1 sec. Configuration h.

Fig. 8d. Powder concentration for 5 µm particles at 0.2 sec. Configuration h.
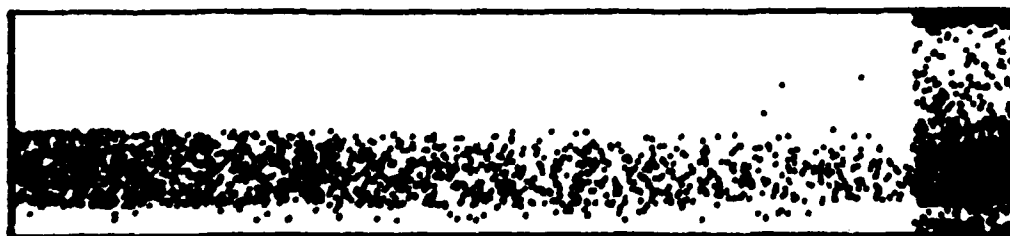
Fig. 8e. Powder concentrations for 200 μm particles at
0.1 sec. Configuration i.
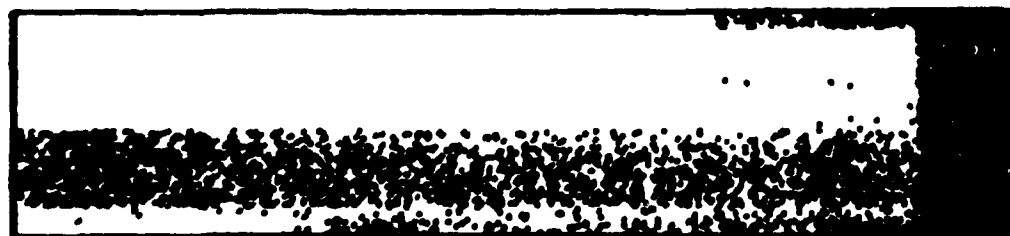
Fig. 8f. Powder concentrations for 200 μm particles at
0.2 sec. Configuration i.

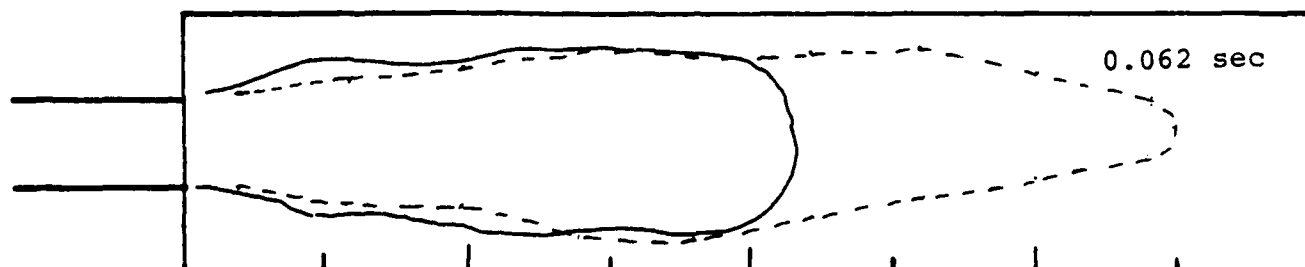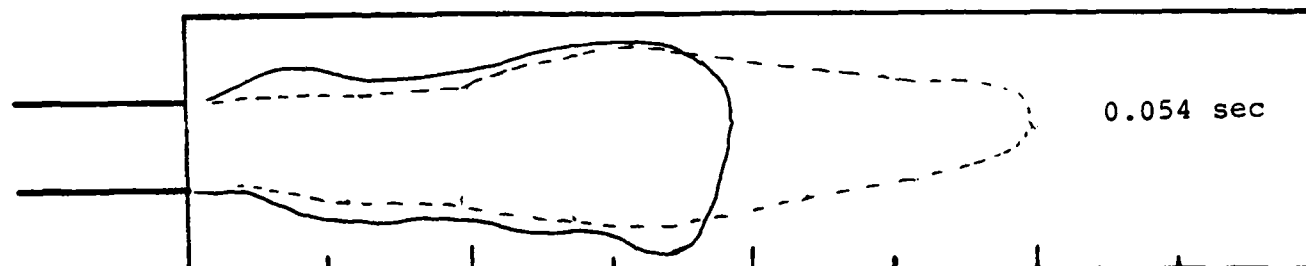Figure 8. EFFECT OF PARTICLE SIZE ON POWDER VOLUME
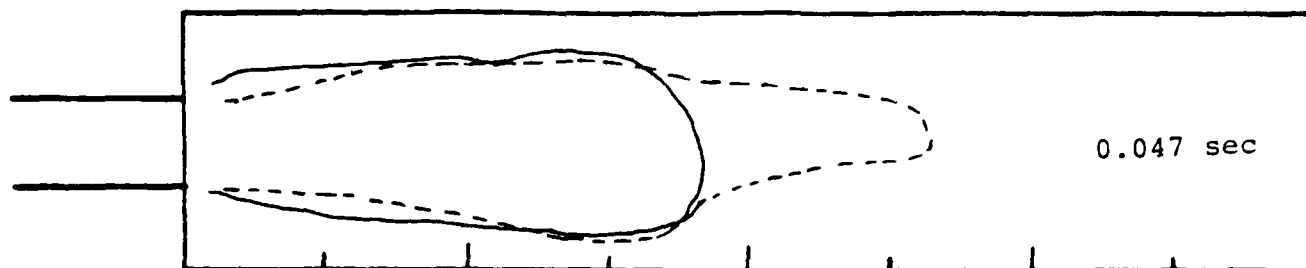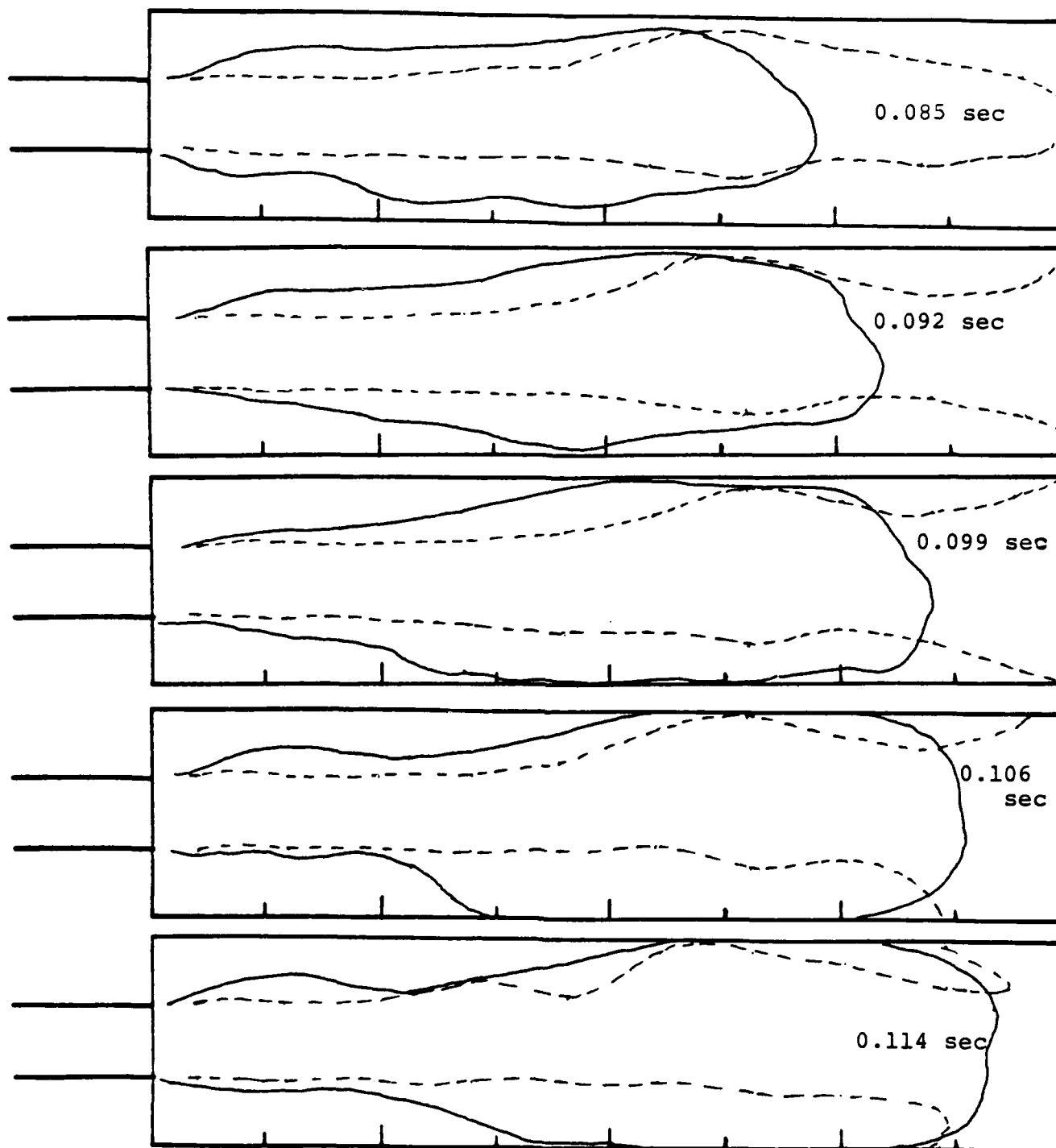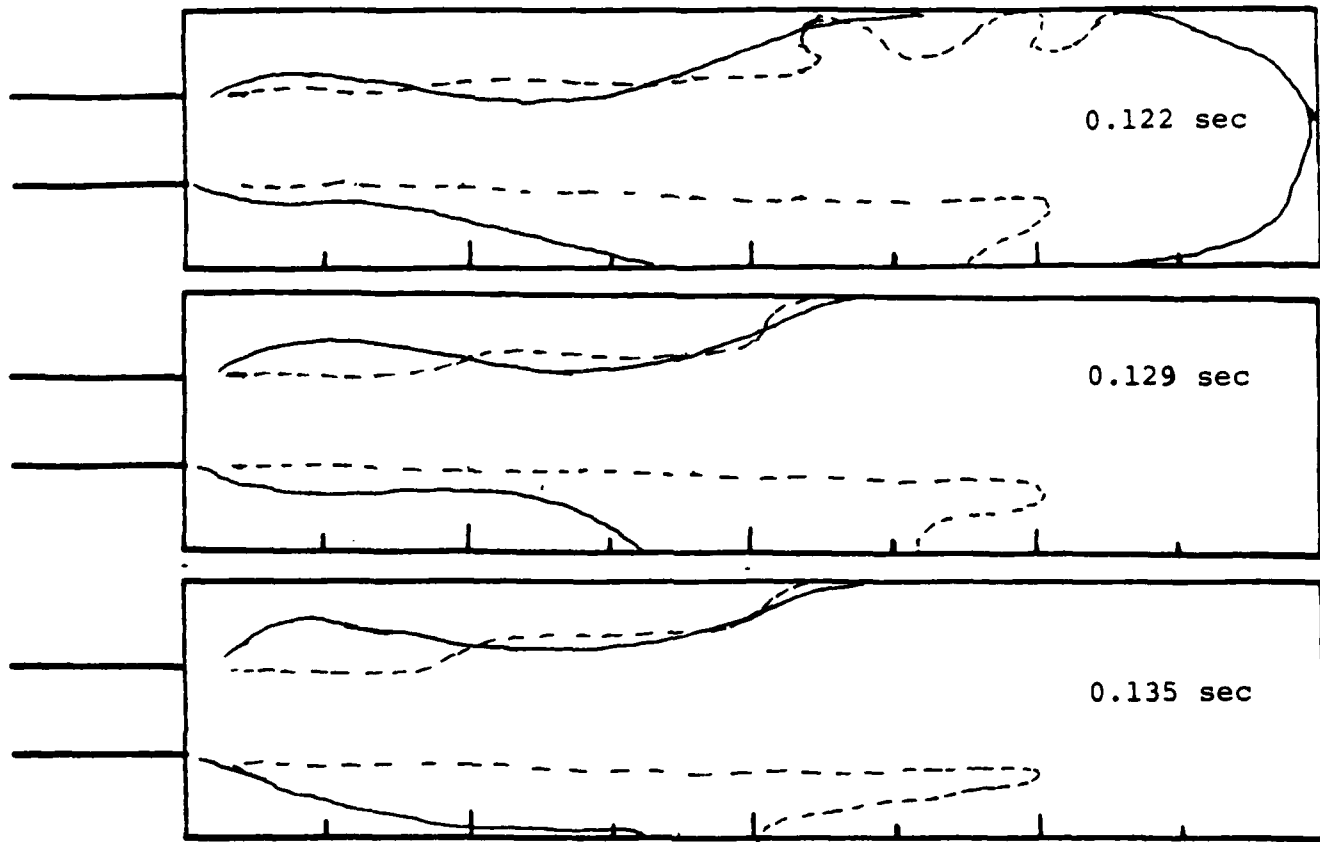FRACTIONS.
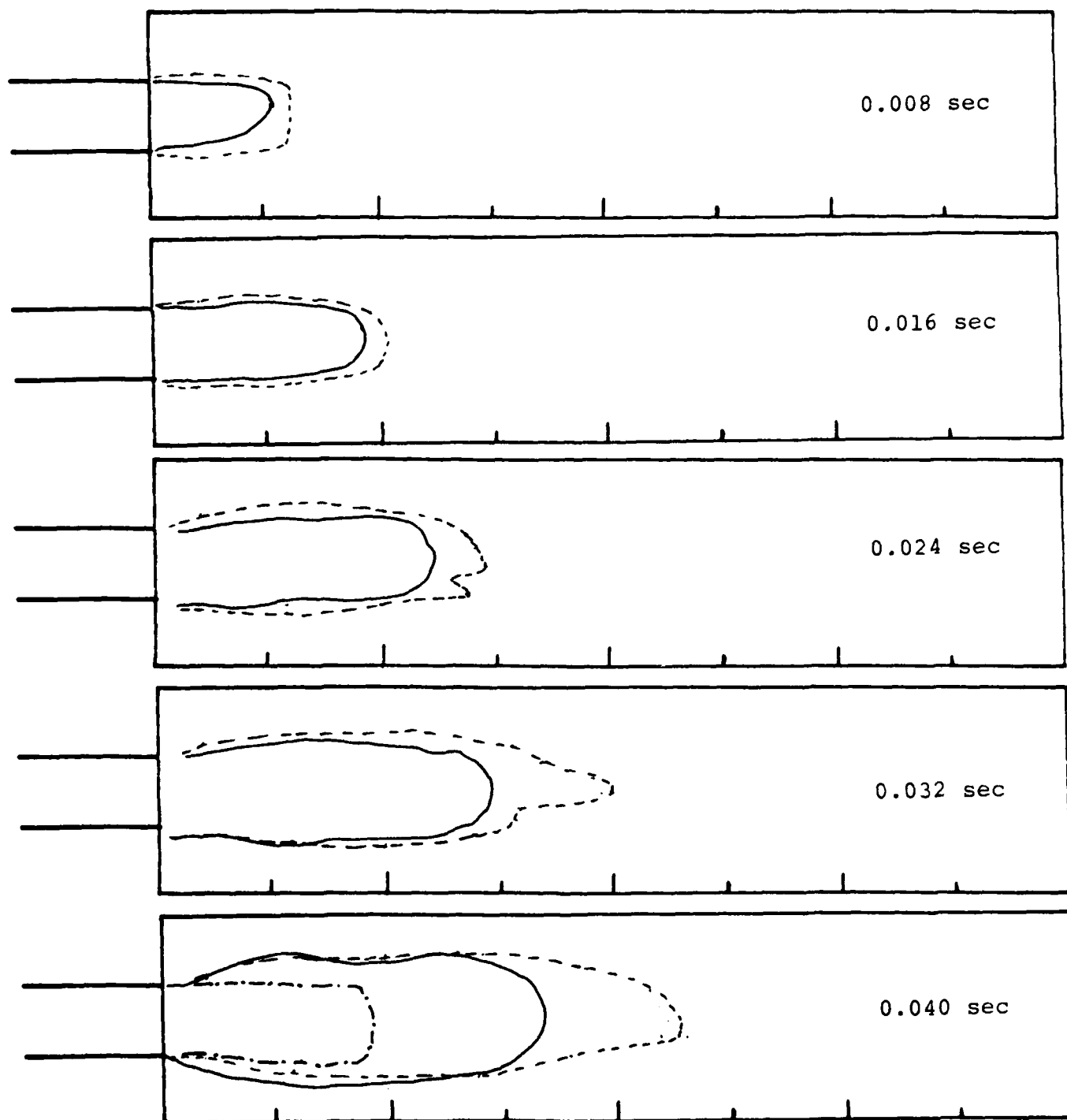
Figure 9. Comparison of Computed (configuration k) and Experimental (Run BM-4) Concentration Profiles at Various Times (Seconds) after Injection. Solid Line-Experimental. Dashed-Volume Fraction of Solids of $2x10^{-4}$ Dot-Dash-Computed Volume Fraction of $18x10^{-4}$.

0.047 sec

0.054 sec

0.062 sec

0.070 sec

0.078 sec

0.085 sec

0.092 sec

0.099 sec

0.106
sec

0.114 sec

0.122 sec

0.129 sec

0.135 sec

END

FILMED

7-80

DTIC